MOUNTAIN-PLAINS CONSORTIUM

MPC 15-280 | K. Ng, R. Ettema, E. Kempema, R. Chakradhar, and J. Fuller

Geotechnical Limit to Scour at Spill-through Bridge Abutments: Laboratory Investigation

A University Transportation Center sponsored by the U.S. Department of Transportation serving the Mountain-Plains Region. Consortium members:

Colorado State University
North Dakota State University
South Dakota State University
University of Colorado Denver
University of Denver
University of Utah
Utah State University
University of Wyoming

Geotechnical Limit to Scour at Spill-through Bridge Abutments: Laboratory Investigation

Kam Ng, PhD, PE
Robert Ettema, PhD, PE
Edward Kempema, PhD
Ram Chakradhar
Joshua Fuller

Department of Civil and Architectural Engineering
University of Wyoming
Laramie, WY

March 2015

Acknowledgements

The authors thank the Mountain-Plains Consortium for funding the present project, MPC Project 14-354, *Geotechnical Limit to Scour at Spill-through Abutments*. This project's principal investigators were Robert Ettema and Kam Ng. They were assisted by two graduate students, Josh Fuller and Ram Chakradhar, who completed master's degree theses as part of the project. Research engineer Ed Kempema assisted with the conduct of the flume experiments and analysis of observations and data.

ABSTRACT

Scour of spill-through abutments occurs due to the combined influence of geotechnical and hydraulic processes. The present study is among the first to address the geotechnical process associated with the failure of the compacted earth, spill-through abutments, and the effects of the geotechnical strength of spill-slope soil on abutment scour. Laboratory experiments were completed to determine how soil shear strength affects abutment scour. The experiments, which primarily involved sand compacted to varying strengths, and some clayey soils, led to new and useful insights. A major new finding is that abutment failure begins at the water line of the spill-slope's upstream corner, where flow constriction around an abutment exposes and erodes spill-slope soil to the highest values of flow velocity and turbulence. Once initiated, erosion continues toward the middle portion of the spill-slope face, and then progresses downstream. Spill-slope erosion is marked by the formation of undercut, exposed vertical blocks of embankment soil whose failure occurred relatively quickly once the spill-slope face began eroding. Abutments formed of stronger soils took longer to erode, had bigger blocks of failed soil, and produced deeper scour of the channel around the abutment. Rapid failure of an abutment resulted in shallow scour depths.

TABLE OF CONTENTS

LIST OF FIGURES

LIST OF TABLES

LIST OF ABBREVIATIONS

ASTM	American Society for Testing and Materials
CH	High plasticity clay
CIMCPT	Continuous Intrusion Miniature Cone Penetration Test
CL	Low plasticity clay
COFS	Center for Offshore Foundation System
CPT	Cone Penetration Test
CPT_u	Piezocone Penetration Test
DOT	Department of Transportation
DST	Direct Shear Test
FDOT	Florida Department of Transportation
FHWA	Federal Highway Administration
HEC-18	Hydraulic Engineering Circular -18
LL	Liquid Limit
MCPT	Miniature Cone Penetration Test
MDD	Maximum Dry Density
MH	Inorganic Silt with high plasticity
ML	Inorganic Silt with low plasticity
MPC	Mountain Plain Consortium
NCHRP	National Cooperative Highway Research Program
NHI	National Highway Institute
OH	Organic silt with high plasticity
OL	Organic silt with low plasticity
OMC	Optimum Moisture Content
PI	Plasticity Index
PL	Plastic Limit
SC	Clayey Sand
$SCPT_u$	Seismic piezocone test
SP	Poorly graded (or uniform) sand as per USCS
SPT	Standard Penetration Test
UC Davis	University of California Davis
USCS	Unified Soil Classification System
UWA	University of West Australia
WYDOT	Wyoming Department of Transportation

LIST OF SYMBOLS

Θ_s	Maximum slope
c	Cohesion
C_c	Coefficient of curvature
C_u	Coefficient of uniformity
D_{10}	Grain diameter at 10% passing
D_{30}	Grain diameter at 30% passing
D_{60}	Grain diameter at 60% passing
D_r	Relative density
d_{smax}	Maximum scour depth
E_H	Embankment height
e_{max}	Maximum void ratio
e_{min}	Minimum void ratio
f_s	Sleeve friction
q_c	Tip resistance
q_u	Unconfined compressive strength
R	Penetration resistance
r^2	Correlation coefficient
S_u	Undrained shear strength
U	Porewater pressure
γ	Unit weight
γ_d	Dry unit weight
γ_{dmax}	Maximum dry index unit weight
γ_{dmin}	Minimum dry index unit weight
σ_v	Normal stress
τ	Shear strength
ϕ	Friction angle

ASTM STANDARDS

ASTM 421 (2002)	Standard practice for dry preparation of soil samples for particle-size analysis and determination of soil constants
ASTM D 2573-08 (2008)	Standard Test Method for Field Vane Shear Test in Cohesive Soil
ASTM D 4648 (2010)	Standard Test Method for Laboratory Miniature Vane Shear Test for Saturated Fine-Grained Clayey Soil
ASTM D 698-91 (1992)	Laboratory compaction characteristics of soil using standard effort (12,400ft-lbf/ft^3(600kN-m/m^3))
ASTM D1558-10 (2010)	Standard Test Method for Moisture Content Penetration Resistance Relationships of Fine-Grained Soils
ASTM D2487 (2000)	Standard Practice for Classification of Soils for Engineering Purposes (Unified Soil Classification System)
ASTM D3441 (2005)	Standard Test Method for Mechanical Cone Penetration Tests of Soil
ASTM D422-63 (2002)	Standard Test Method for Particle-Size Analysis of Soils
ASTM D4253 (2006)	Standard Test Methods for Maximum Index Density and Unit Weight of Soils Using a Vibratory Table
ASTM D4254 (2006)	Standard Test Methods for Minimum Index Density and Unit Weight of Soils and Calculation of Relative Density
ASTM E100 (2010)	Standard Specification for ASTM Hydrometers
ASTM-D-5778 (2012)	Standard Test Method for Electronic Friction Cone and Piezocone Penetration Testing of Soils

1. INTRODUCTION

1.1 Introduction

The findings of this study show that scour at spill-through abutments involves geotechnical and hydraulics erosion processes, and confirm that geotechnical failure of abutment spill-slope limits scour depth. Observations of failed abutments commonly reveal that the geotechnical failure of the compacted earth spill-slope, and thus the geotechnical strength of the spill-slope, influence the extent, depth, and rate of abutment scour. Abutment failure directly influences scour depths at abutments by increasing the flow area through a bridge opening, reducing flow velocities and producing scour depths less than reported in laboratory studies reported in the literature on scour.

Though numerous illustrations of scour at spill-through abutments show failed embankment and channel bank (e.g., Figures 1.1 and 1.2), the methods currently available for estimating scour do not address the geotechnical aspects of scour at spill-through abutments. The leading design guides and bridge-monitoring guides inadequately characterize scour at bridge abutments. For example, the recent FHWA publication HEC-23 by Lagasse et al. (2009) and the FHWA design guide HEC-18 by Richardson and Davis (2001) inadequately describe abutment scour.

The main contributions of this study are the characterization of failure mechanics of embankment soil and determination of soil strength effects on the scour development and total scour depth. These contributions are based on the findings from novel laboratory flume experiments conducted with a 1:30-scaled model using sand, clayey sand, and a sand clay mixture compacted as embankment to achieve arrays of strength for each soil. The strengths of the model embankment soil used in the flume experiments were predicted by correlating them against the laboratory tests of model soil properties. In particular, the main experiments involved controlled compaction of uniform sand in order to control the sand's shear strength.

The practical outcome of this study is substantially improved understanding of scour at spill-through abutments, including new insight into how abutments fail. This information is needed for efficient and safe abutment design and maintenance. As embankment failure is a common aspect of bridge failure at bridge waterways, the study's findings will help enhance the stability of bridge abutment for the smooth operation of traffic.

Conduct of this study involved two graduate students, Joshua Fuller and Ram Chakradhar, who completed master's degree theses during the term of the study (Fuller 2012 and Chakradhar 2014).

In addition, the study addresses important aspects of the following specific principal goals associated with the Mountain Plains Consortium (MPC) Program and U.S. Transportation Board, generally:

- Infrastructure longevity (better abutments)
- Improved infrastructure design (better and safer abutments)
- Environmental impacts of infrastructure (effect of abutment on flow and erosion)
- Low-cost safety improvements (effective placement of scour countermeasures)

Figure 1.1 Abutment failure due to scour attributable to geotechnical failure of spill-slope

Figure 1.2 Bridge abutment column standing after spill-slope failure

1.2 Objectives and Scope

This study had the following research objectives:

1. Understand and describe the scour failure of spill–through abutments in terms of the combined effect of the geotechnical and hydraulic processes contributing to it;
2. Analyze failure mode of embankment slopes;
3. Determine how embankment soil strength (at least for the soil conditions tested) influences the extent, depth, and rate of scour at spill-through abutments;
4. Develop an in-situ soil testing procedure to estimate embankment soil's shear strength for a scaled down model and,
5. Outline the necessary methods and difficulties of conducting hydraulic model laboratory experiments involving combined geotechnical and hydraulic erosion processes.

The scope of the experiments was mainly limited to the strength of compacted uniform sand embankments and its effect on scour depth. However, preliminary additional experiments were also carried out using cohesive soil (clayey sand) and mixture of sand and clay.

1.3 Report Organization

Five main research tasks were performed, and are reflected by the organization of this report:

1. **Literature Review:** A literature review was performed to understand the background of bridge failures relating to scour. Factors influencing bridge abutment failure, theories that explain the failure mechanism, and design guides recommended by the Federal Highway Administration (FHWA), National Cooperative Highway Research Program (NCHRP), and Wyoming Department of Transportation (WYDOT) were reviewed. Literature review pertinent to the geotechnical factors associated with the stability of the embankment and its effect on scour were conducted and arranged in 0: Literature Review.

2. **Measurement System for Soil Properties:** Several measurement systems were investigated to measure the soil strength parameters before and during the flume test. The measurement systems are direct shear test, pocket penetrometer, torsional vane shear test, and miniature Cone Penetration Test (CPT). Soil strength parameters, such as cohesion and friction angle, are important properties in quantifying soil shear strength achieved during compaction and placement in the flume that will ultimately help in determining the relationship between soil strength and scour depth. Rigorous search for the instruments by contacting different geotechnical companies, consultants, professionals, and researchers in the field were carried out and documented. This task is briefly explained in 0: Measurement Systems for Soil Properties.

3. **Laboratory Soil Testing:** A comprehensive laboratory soil testing was performed to characterize all the soil used in the flume experiments. The laboratory soil tests comprise sieve analysis, Atterberg limit tests, soil classifications as per Unified Soil Classification System (USCS), standard Proctor compaction tests, direct shear tests, torsional vane shear tests, and shear tests using pocket penetrometer. In this task, sets of standard soil properties were determined for each soil type (i.e., cohesive, cohesionless, and mixed soil). The laboratory test results are reported in 0: Laboratory Soil Testing.

4. **Flume Experiments:** Flume experiments carried out were set up to a scale of 1:30 to simulate the actual field condition. Three different soil types (cohesive, cohesionless, and mixed soil) were used as model embankment for three different sets of experiments. 0 explains the experimental set-up and

arrangements, procedures followed, parameters used, and the data collection methods under the heading Flume Experiments.

5. **Analysis and Discussion of Results:** Systematically recorded data during flume experiments and time lapse photographs were analyzed to investigate the trend and develop a relationship. The illustrations of experiments using different model soil abutment and the computation of analysis parameters are also discussed in this task, whose results are presented in 0: Analysis and Discussion of Results.

6. **Conclusions and Recommendations:** Recommendations and conclusions of the research are reported in a manner that is useful for bridge engineers. The significance of the research was highlighted and potential future research works were recommended; this is arranged in 0: Conclusions and Recommendation

2. LITERATURE REVIEW

2.1 Introduction

About 84% of the bridges in the United States are over waterways (Landers 1992), and are prone to failure owing to waterway scour. Among the 86 bridges that failed during 1961 to 1976, for example, far more abutments failed due to scour than to earthquakes, wind, structural problems, corrosion, and automobile accidents combined (Murrillo 1987). These numbers indicate the substantial significance of scour as a concern for bridge design. Yet, although numerous research articles address the hydraulic aspects of abutment scour, scant few have addressed the importance of geomechanical aspects associated with scour estimation. This section briefly reviews the literature regarding geotechnical processes involved in abutment scour.

2.2 Existing Knowledge on the Geomechanics Aspects of Scour

As the geomechanical aspects associated with abutment scour have not been explored much, the extent of existing literature on this aspect of scour is notably very limited. The most developed effort to consider geotechnical effects is the conceptual method proposed by Ettema et al. (2010) to estimate the maximum scour depth limited by the geotechnical stability of channel bank and earthfill approach embankment.

The method proposed by Ettema et al. (2010) is shown in Figure 2.1. It is the only method presently available that considers the coupled interaction of geotechnical and hydraulic process causing abutment scour. Ettema et al. (2010) state that hydraulic process initiates scour, with the depth and lateral extent of scour being influenced by erosion of the channel bank and abutment's embankment. They suggest that a simple estimation of scour depth at an abutment can be made using equation (2.1), which assumes a maximum slope angle, θ_s, for stability of abutment splill-slope; i.e.,

$$\theta_s = \tan^{-1}\left(\frac{E_H + d_{smax}}{R}\right) \tag{2.1}$$

where, E_H is the embankment height and R is the distance from embankment top to the location of maximum scour depth. This equation estimates limiting values of maximum scour depth d_{Smax} as,

$$d_{smax} = R \times \tan(\theta_s) - E_H \tag{2.2}$$

However, the foregoing formulation is conceptual and lacks verification by means of laboratory experiments. Such experiments have not yet been conducted to verify this formulation in part because of the complexity of laboratory simulation of combined geotechnical and hydraulic process. In particular, other than the work by Fuller (2012), no prior work has considered laboratory scaling of soil strength. However, the study by Fuller (2012) was preliminary in nature, and resulted in an inconclusive quantitative relationship between soil strength and scour depth.

Current scour estimation methods estimate potential values of scour depth based only in terms of hydraulic considerations that could be applicable only if an abutment did not fail (e.g., Sturm et al. 2012). Although Sturm et al. (2012) acknowledge the likely significance of abutment soils strength on scour depth, they do not indicate how it should be included in estimates of scour depth. No other study on abutment scour addresses how abutment soil influences scour depth (e.g., Melville and Coleman 2000).

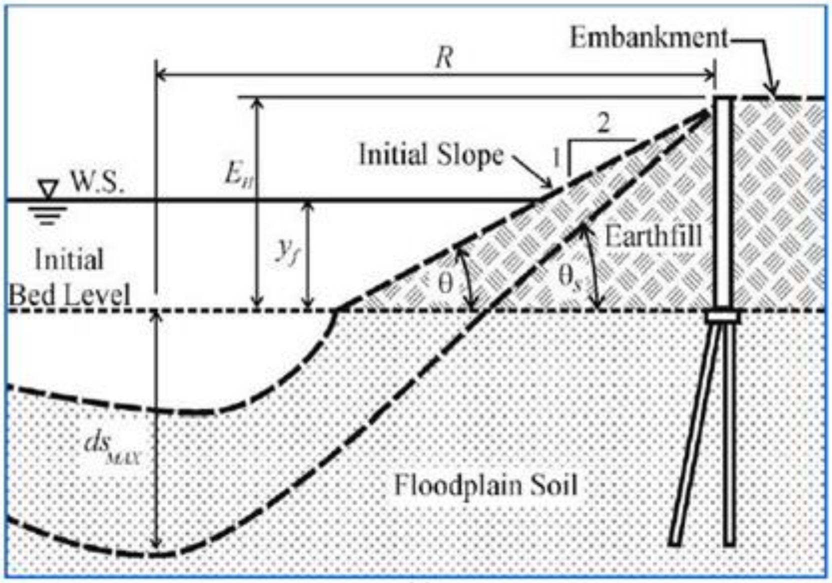

Figure 2.1 Scour depth estimation based on geotechnical stability of embankment (Ettema et al. 2010)

To estimate scour depth with reasonable accuracy, it is necessary to estimate abutment soil strengths, and include this estimate in a comprehensive formulation of scour and abutment failure. Prevailing design practice, for example in HEC-18 (Arneson et al. 2012), mentions that the engineering properties of soil at bed and bank resist scour, but offer little insight as to how soil strength should be included in estimates of scour depth. None of the scour depth estimation equations take into account embankment soil geotechnical properties (e.g., Sturm et al. 2012).

Therefore, the current state of practice lacks information regarding how bridge abutments fail, and how failure is influenced by abutment soil strength, rate of abutment spill-slope erosion, and the extent of spill-slope erosion. In the only study to date, Fuller (2012) concludes that a toppling failure of discrete blocks of embankment soil occurs due to undercutting by flow erosion. His findings, based on flume experiments, comprise a precursory study to the present study. He showed, from flume experiments, that abutment scour depth is affected by abutment soil shear strength; with clay soils, by virtue of their greater strength, causing the higher scour depth compared with other erodible soils. He observed the combined effects of hydraulic and geotechnical erosion processes during flume experiments, and reported they occurred as a cycle of under-cutting, tension-crack formation, and toppling failure of model soil into the flow. Eventually the spill-slope eroded back sufficiently so as to cause the average velocity of flow through the waterway to reduce, hence scour of the floodplain attained an equilibrium depth and no longer deepened.

2.3 Abutment Erosion as a Form of Riverbank Erosion

Erosion of a bridge abutment can be viewed as a form of riverbank erosion, and likely involves essentially the same combination of hydraulic and geotechnical processes. Bank failure occurs in several forms, but typically involves the formation of tension cracks a few feet back from the bank line. The process entails a slab-type rotational failure; a combined process of planar and toppling failure (e.g. Hossain et al. 2010).

As for erosion of a bridge abutment, riverbank erosion and failure are influenced by the geotechnical strength properties of their soil, and by the erosive shear stress of flow. The failure of cohesive riverbank soils usually is attributable to several factors (e.g., Osman and Thorne 1986), including:

- lateral erosion by channel widening that steepens the bank
- bed lowering that increases the bank height and decreases stability

These processes are influenced by the soil strength parameters, notably soil cohesion and friction angle. Additionally, as indicated by several studies (e.g., Osman and Thorne 1986), the rate of lateral erosion of a bank formed of a cohesive soil is influenced by the soil's physical and chemical makeup. For instance, an increase in a soil's shear resistance can be associated with an increase in clay content or decrease in sodium ions in soil. Osman and Thorne (1986) present a practical method for predicting riverbank stability based on bank geometry (slope, height, and cut bank critical height) and a set of parameters influencing soil strength (effective cohesion, effective friction angle, and bulk unit weight). Use of this method is beyond the scope of the present study, but the method (and possibly similar other advanced methods) could be implemented in future studies.

Although the present study has not exhaustively reviewed the extensive amount of research that has been devoted to riverbank erosion, the information presented here indicates excellent promise for exploring the analogy between erosion and failure of abutments and riverbanks, especially regarding curved riverbanks.

2.4 Conclusions

The present review of the meager amount of literature addressing geotechnical processes contributing to abutment scour and failure reveals that there is indeed a major gap in knowledge about these processes. Therefore, the present study is an early attempt to explore influence of abutment soil shear strength properties on abutment scour and failure, including how soil strength influences the rate of spill-slope erosion.

Evidently, the leading scour estimation and bridge design guides do not adequately address the processes, and therefore offer design estimations for scour depth that should be treated as being conservative, because they do not consider abutment erosion. Besides the study by Fuller (2012), no prior study incorporates soil strength considerations in descriptions of abutment scour and failure. However, Fuller (2012) was unable to show a quantitative relationship between abutment soil strength and scour depth. Although numerous field case examples show that abutments fail during abutment scour, it is remarkable that no design methods (other than Ettema et al. 2010) have attempted to take geotechnical factors into consideration when describing and estimating abutment scour. This review has indicated that excellent prospects exist for applying concepts of riverbank erosion to abutment erosion; an abutment, after all, is a form of convexly curved riverbank.

3. MEASUREMENT SYSTEM FOR SOIL PROPERTIES

3.1 Introduction

A substantial challenge for this study was to determine the shear strength of different soil types used in flume experiments. The relatively small size and modest thickness of the model abutments used for the flume experiments complicated the accurate measurement of soil strength. This challenge was addressed by development of an indirect approach using the instruments described in this section.

Because soil strength is significant in determining the overall performance and stability of embankment slope, as well as in co-relating scour in terms of soil strength, determination of shear strength of embankment soil was a key aspect of this study. However, a standard device was not available to predict the strength of model soil used to form the small size model spill-slope abutment. Actual in-situ soil testing equipment is intended for, and works best with, thick soil formations. A significant task of this study entailed investigating if customized in-situ test equipment exists for a precise measurement of soil shear strength in small-scale laboratory models of soil formations such as road embankments and slopes.

The investigation led to a four-part in-situ soil testing procedure, as described in this section. The procedure is based on use of a needle penetrometer for correlating the model soil (sand) properties. Although Mini Cone Penetration Test (Mini CPT) equipment was not used in the present flume experiments, the investigation indicated that it could be applicable for future use if a personalized, inexpensive mini CPT device became available. Additionally, the investigation compared the use of a hand-held pocket penetrometer and a torsional vane shear tester. This comparison found that the torsional vane shear tester was more useful for the flume experiments.

The ensuing sections of this section describe the findings of the investigation, and outline of the soil-testing procedure adopted for the present study.

3.2 Needle Penetrometer

A needle penetrometer consists of a spring-loaded plunger with a needle attached to its end as shown in Figure 3.1. A set of needles with various end areas is available to facilitate the measurement of wide range of penetration resistances. The penetrometer has a sliding ring attached to a graduated stem that slides vertically when needle is pushed through the sample. It measures the distance of penetration (penetrometer reading) into the soil, and the penetration resistance can be correlated to the shear strength of the tested soil.

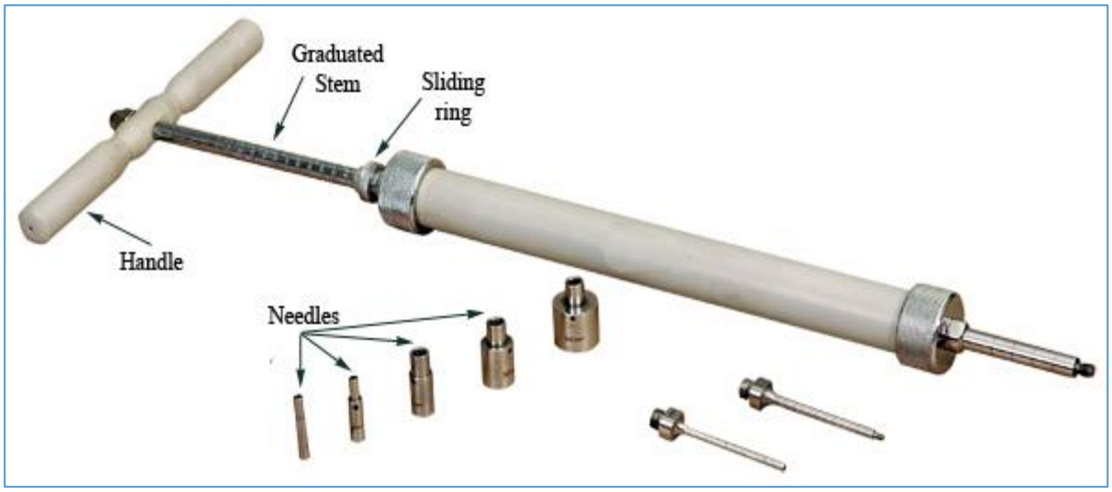

Figure 3.1 Needle penetrometer

The needle penetrometer was used to determine the penetration resistance of sand and sand-clay mix at different densities in this research. Needles with different end areas were used for the sand compacted at various relative densities (D_r). The penetration is carried out at the rate of 13 mm/s (0.5 in/s) for a penetration depth not less than 76 mm (3 in). At least three measurements were taken during the laboratory tests to obtain an average penetration reading while five measurements were taken on each compacted uniform sand and sand-clay mix embankments in flume experiments. This average reading when multiplied by the reciprocal of end area of the selected penetration needle gives the penetration resistance. Although the needle penetrometer test performed in accordance with the ASTM D1558-10 (2010) was developed for fine grained soil, this test procedure was adopted for sand to determine penetration resistance as an index of controlling relative densities in the flume experiments. The test procedure of pushing a needle into sand (or clay sand mix) is an analogy to pushing a cone penetrometer during a CPT or a split-spoon sampler into sand during a Standard Penetration Test (SPT). Using this analogy, it is justifiable to adopt the needle penetrometer test on sand and sand-clay mix. Additionally, consistent penetration resistances of sand as shown in Figure 4.2 were obtained, indicating the reliability of this test method on sand. Knowing the relative density of sand, its in-situ shear strength in the flume can be determined based on a correlation established between the relative densities and shear strength measured from a series of direct shear tests performed as discussed in Section 4.

3.3 Cone Penetration Test (CPT) Device

3.3.1 Introduction

The Cone Penetration Test (CPT) is a reliable, fast, and economical method of non-disruptive soil testing that is widely used by engineers working on transportation-related projects. According to National Cooperative Highway Research Program (NCHRP) Synthesis 365 (Mayne 2007), out of 56 departments of transportation (DOTs) who responded the survey, 27% used CPT on a regular basis, 36% only used it on about one-tenth of their projects, and the rest (37%) do not use CPT at all. The survey results also recorded that 64% of the DOTs planned to increase their use in the future.

Soil profile, tip resistance (q_c), sleeve friction (f_s), and pore water pressure (u) can be obtained using CPT in accordance with ASTM-D-5778 (2012) based on electric and electronic systems and ASTM D3441 (2005) based on mechanical systems. Standard CPT Equipment consists of a cone-shaped penetrometer that is pushed into the soil using an external loading cell at a rate of 20 mm/s and a reading is taken at an interval of 10 or 50 mm. The conical tip is inclined at 60^0 at the apex. It is also equipped with a friction sleeve of 150 cm^2 surface area to measure the friction between the soil and shaft of probe. CPT is capable of measuring soil properties at a depth greater than 30 m. Using an electronic steel probe connected with a data acquisition system, the output can be automatically recorded in a computer.

A variety of cone penetrometer systems is available, ranging from small hand-held, mini pushing units to very large truck and track-mounted vehicles. The electronic penetrometers range in size from small to large probes, from one to five separate channels of measurements (Mayne 2007).

3.3.2 Types and Uses of Cone Penetration Test (CPT)

A Continuous Intrusion Miniature Cone Penetration Test system (CIMCPT) uses a projected cone area as small as 2 cm^2. According to research (Kurup and Tumay 1998), the Miniature Cone Penetration Test (MCPT) gives a finer detail than the standard 10 cm^2 cross-sectional area cone penetrometer, which makes it the best fit for geotechnical assessment of embankment or subgrades in transportation. The piezocone Penetration Test (CPT_u) uses penetrometers with added transducers for porewater pressure measurements. Seismic piezocone Test ($SCPT_u$) has an advantage of measuring shear waves to determine the soil stiffness. Resistivity piezocone, which has electrical conductivity or resistivity readings, facilitates the detection of freshwater-salt water interfaces.

3.3.3 Applicability to flume tests

For the 0.2m-thick (0.66 ft), shallow depth, model embankment in flume experiments, the mini cone with reduced diameter was found to be effective (though not used in this research) to determine the shear strength of embankment soil. The CPT probe has to be sensitive enough to measure the low friction and tip resistance. A standard cone would not be able to record, or the recorded value will be unrealistic if measured (quoted by Dr. Baxter in email). Although customized mini CPT would have been beneficial to the flume experiment, it was not available for the present study.

3.3.4 Search for mini CPT with smaller diameter

The miniature piezocone has been used in a typical centrifuge testing of soil properties and has proven to give reliable and consistent measurements of soil properties (Esquivel and Silvia 2000). Several geotechnical companies were contacted to find a mini CPT for possible use in the flume experiments. A number of university professors and industry professionals in the geotechnical field who have expertise working with mini cone and soil testing were contacted. Eventually, a useful recommendation was received by email from Dr. Mehmet T. Tumay, a retired professor from Louisiana State University. He recommended contacting Greggdrilling & Testing Inc., based in South California.

Also, it was found that a program of geotechnical centrifuge testing carried out at the University of California (UC) at Davis for soil properties uses a mini CPT to measure the strength of soil samples. Prof. Jason Dejong from UC Davis said 6 mm diameter CPTs they developed with pore pressure is not robust. He advised, in an email response, to contact Fugro for the instrument.

Another contact stated in an email reply: "The effective stresses and tip resistance that would be measured in the flume experiment would be very low and a true cone with tip and sleeve friction won't be able to accurately measure it." Professor Chris Baxter from the University of Rhode Island has used a 1 cm^2 piezocone manufactured by Fugro in a calibration chamber with some successes (Baxter et al. 2010).

However, contrary to the recommendations from Dr. Tumay and Professor Baxter, Fugro, based in Houston, Texas, responded they don't manufacture mini cones. Also, Greggdrilling & Testing Inc.

responded that they do not sell their mini cones, which usually are used for offshore investigations. Furthermore, John Flynn from GeoKon Inc., Carl Tracy from Vertek, and Sue Jones from Olson Instruments Inc. replied that their mini CPTs cannot be used for soil thicknesses less than 0.5m (1.64ft).

After an extensive investigation, the price quotations were received from two companies, Center for Offshore Foundation System (COFS) at University of West Australia (UWA) and A.P. van den Berg (Netherlands). What COFS offered was more specific to the CPT used in Centrifuge testing, and was costly. The offer from A.P Van Den Berg was somewhat more reasonable in cost. A.P Van Den Berg offered a 2 cm^2 cone that can be collaborated with an external pusher system and the Campbell Scientific CR 1000 data acquisition system for recording data. It was decided not to use CPT devices for the flume experiments as the purchasing price exceeded the project's budget.

3.4 Pocket Penetrometer

3.4.1 Introduction

A Pocket Penetrometer, as shown in Figure 3.2, is a hand-operated soil penetration device used to determine the unconfined compressive strength. It consists of a 6.35 mm (0.25 in) diameter piston that is manually pushed into the soil with a vertical force at a distance of 6.35 mm (0.25 in). The indicating ring around the calibration is set to zero before the test. It slides along the reading when the device is being pushed into the test soil until the calibration mark as indicated in Figure 3.2 at the tip of piston is leveled with the soil. The reading on the scale directly gives an unconfined compressive strength (q_u) in kg/cm^2. The undrained shear strength (S_u) can be calculated as $\frac{q_u}{2}$.

This instrument is suitable for cohesive soil. For soil with low or no cohesion, such as sand, an adapter foot with a larger diameter of 25 mm (1 in) is connected to the tip of device during penetration. The recorded value of unconfined compressive strength has to be divided by 16 to yield the actual value of strength in order to account for the adapter foot calibration correction.

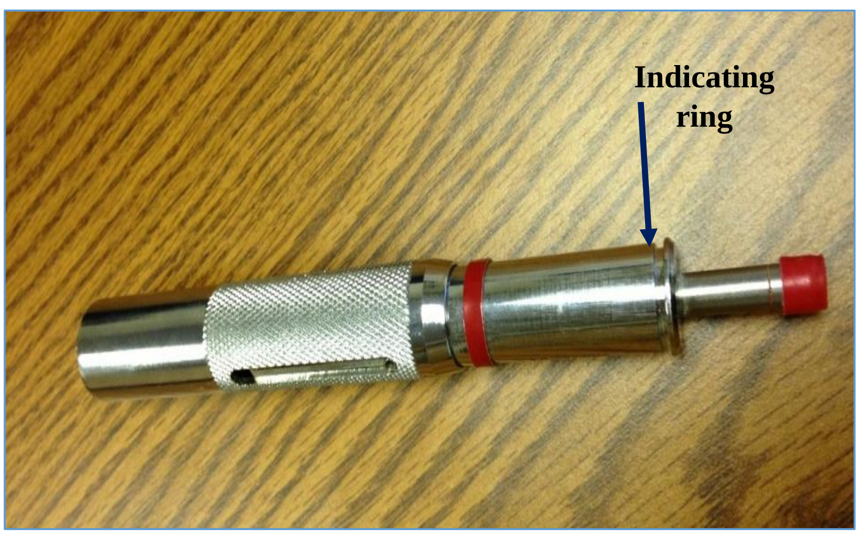

Figure 3.2 Pocket penetrometer

3.4.2 Applicability to flume experiments

In spite of being a readily usable method for determining soil shear strength, the accuracy of the hand-held penetrometer test depends on the skill of an operator and test location where the piston is being pushed. Although used in many applications, tests using a hand-held penetrometer are usually not considered a standard test method for determining soil strength.

The Florida Department of Transportation (FDOT) (2000) considered using a pocket penetrometer and miniature vane shear (Torvane) only for a relative measurement of undrained shear strength (S_u) for clay samples (Howard and Badran 2011). The shear strength obtained from this device can't be used for a design purpose. No ASTM standards have been developed for the pocket penetrometer. As of April 2013, no draft has been filed though ASTM committee D18. It is still being evaulated as an open item referred to as WK27337. New Test Method for Pocket Penetrometer Test. Hence, it can only be used to estimate the relative strength of cohesive soils.

In this study, the hand-held Penetrometer tests were carried out on cohesive soil at different percentages of compaction during laboratory tests. A correlation between the percent compaction (dry densities and moisture content) and undrained shear strength (S_u) was developed, which was used to control the percent compaction in the flume experiment. A precaution was taken not to test the soil too close to the edge of proctor mold, which would otherwise over-estimate the strength of the soil due to the boundary confinement.

3.5 Torsional Vane Shear Tester

3.5.1 Introduction

The torsional vane shear tester, as shown in Figure 3.3, is a simple hand-held device used to determine the undrained shear strength of a cohesive soil in the laboratory as well as in the field. It consists of vanes, which are inserted into the soil during testing (Figure 4.17), and torque applied with a constant vertical pressure until the soil sample fails. The circular reading at the top consists of an attached dial, which locks at a position when rotation eases. The division in the circular reading gave the shear strength of soil; the smallest reading being 0.05 kg/cm^2. A number of tests can be performed simultaneously on a same soil sample.

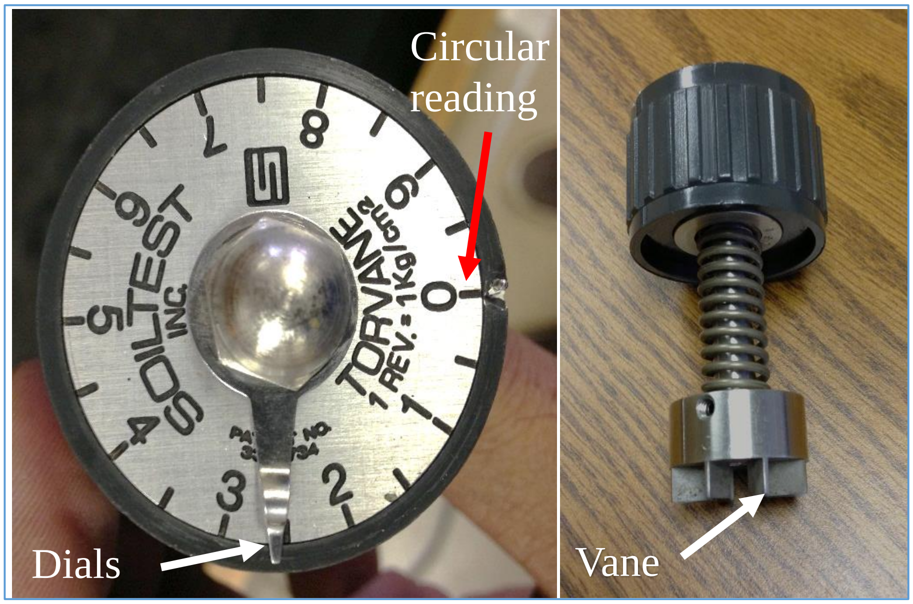

Figure 3.3 The torsional vane shear tester used for this study

3.5.2 Applicability to flume experiment and limitations

The vane shear tester can be used to quickly and conveniently determine the shear strength of a compacted cohesive soil in laboratory and flume. ASTM D 2573 (2008) describes a test method for field vane shear testing in cohesive soils, while ASTM D 4648 (2010) describes a laboratory miniature vane shear test for soft to stiff saturated fine-grained clayey soils with undrained shear strengths less than 1 kg/cm^2. A correlation was developed between the undrained shear strength and cohesive soil compaction in lab using torsional vane shear. The correlation chart developed in Section 4, based on a series of laboratory soil tests, was used to relate the percent of soil compaction in the flume to its undrained shear value.

3.5.3 The pocket penetrometer versus the torsional vane shear

For the flume experiments, the torsional vane shear tester was used in preference over the pocket penetrometer device due to the consistency of the tester in determining soil shear strength. The vane shear tester gave better precision, as illustrated, with a relatively larger coefficient of determination (i.e., r^2 = 0.95) than did the pocket penetrometer (r^2 = 0.84). Data obtained using the pocket penetrometer were highly scattered and the measured values were always higher. More detailed results are presented in Section 0

4. LABORATORY SOIL TESTING

4.1 Introduction

This section describes the laboratory soil tests carried out to determine the engineering properties on the following three different soil types used to simulate model embankment soil in the flume.

4.2 Tests on Sand

The following tests were carried out on the sand used for the model embankment:

- particle size distribution
- relative density
- direct shear test

4.2.1 Particle size distribution

Particle size distribution was performed as per ASTM D422 standard (2007) test method for particle-size analysis of soils. Sand samples were screened through a stack of sieves using a mechanical shaker, and the gradation chart was developed as shown in Figure 4.1.

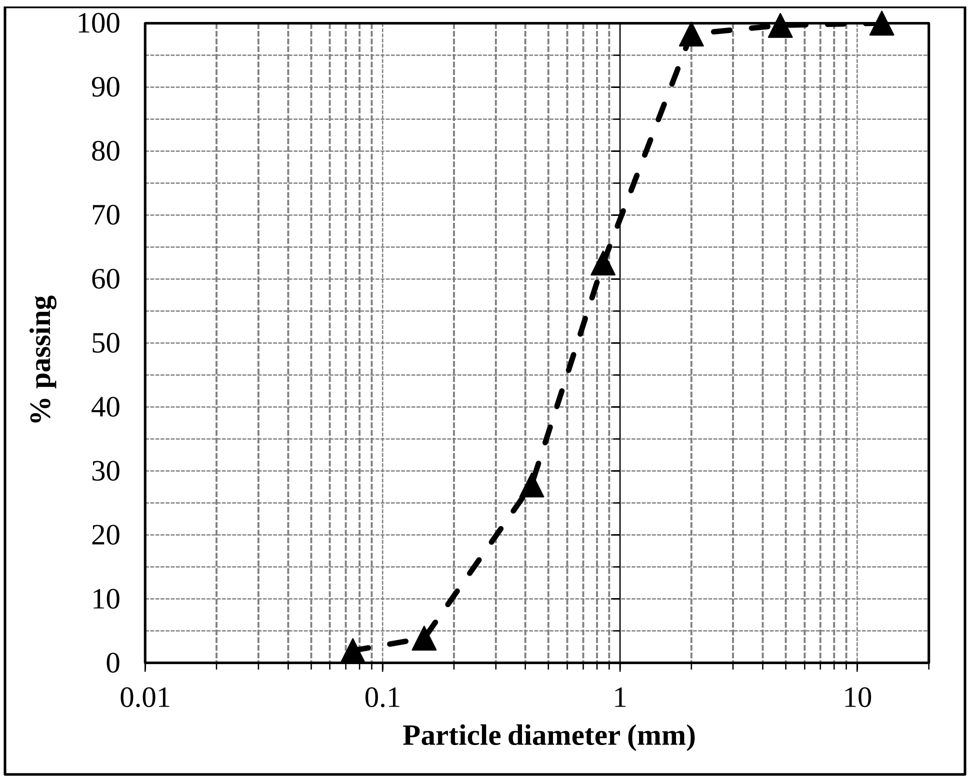

Figure 4.1 The particle size distribution of the sand used in this study

The two shape parameters required to distinguish between well graded and poorly graded sand are coefficient of uniformity (C_u) and coefficient of curvature (C_c). C_u and C_c are given by:

$$C_u = \frac{D_{60}}{D_{10}} \tag{4.1}$$

$$C_c = \frac{(D_{30})^2}{D_{10} \times D_{60}} \tag{4.2}$$

where,
D_{60} = grain diameter at 60% passing,
D_{30} = grain diameter at 30% passing, and
D_{10} = grain diameter at 10% passing

For the sand used in this study, the sieve analysis gave C_u = 4, C_c = 1.3 and the mean diameter, D_{50} = 0.7mm. The detailed calculation of these values was given in Chakradhar (2014) - Appendix A.

4.2.2 Soil classification per the Unified Soil Classification System

From the particle size distribution analysis, it was observed that about 2% passed through sieve no. 200 (0.074 mm), and the percent of gravel was 0.3%. As the C_u value was determined to be less than 6, and the C_c value was between 1 and 2, the sand was classified as poorly graded (uniform) sand with a group symbol (SP). This classification procedure was carried out in accordance with the Unified Soil Classification System, in ASTM Standard D2487. Chakradhar (2014) – Appendix A – presented the detailed calculations.

4.2.3 Relative density of sand

The relative density of sand (D_r) represents its compactness, which affects its engineering properties, notably shear strength, permeability, and compressibility. The test to determine relative density was carried out in accordance with ASTM standards D4253 and D4254. A deviation from the ASTM standard was made while using the mold and applying surcharge load. In this test, a mold with an inside diameter of 152.4 mm (6 in) and height equal to 114mm (4.5 in) was used to determine maximum and minimum index dry unit weights. A 25 kg (55.83 lb) surcharge load was applied while performing maximum index dry unit weight test. Three tests for each (both maximum and minimum) index dry unit weights were performed and the mean index, dry unit weight was then calculated. The average maximum index dry unit weight of the uniform sand used for the study was 17kN/m^3 (108 pcf) at minimum void ratio (e_{min}) 0.53 and average minimum index dry unit weight was 13.9kN/m^3 (88 pcf) at maximum void ratio (e_{max}) 0.87.

Penetration tests using a needle penetrometer were carried out on the same sand samples after relative density tests. Seven sand samples were prepared to attain the unit dry weights between maximum and minimum index dry unit weights. To achieve a series of relative densities, methods from manual tapping on the mold surface using a steel rod to create vibration to changing the total surcharge load during vibration using shake-table were adopted. A minimum of three penetration resistance values on each sand sample prepared were measured. No more than four penetration tests were performed on each sand sample because each penetration would increase the compactness and thereby result in higher resistance to penetration.

Relative density is a relative measure of compactness of sand in reference to the maximum index dry unit weight (100%) and minimum index dry unit weight (0%). A sand sample having a unit weight between the two extreme densities would have a relative density between 0% and 100%. For the present study, the unit weights varied from 13.9kN/m^3 (D_r = 0%) to 17kN/m^3 (D_r =100%). Equation (4.3) was used to calculate relative density.

$$D_r = \frac{\gamma_{dmax}(\gamma_d - \gamma_{dmin})}{\gamma_d(\gamma_{dmax} - \gamma_{dmin})} \times 100\% \tag{4.3}$$

A correlation curve relating penetration resistance (R) and relative density (D_r %) was developed using the penetration test results for a range of relative densities as shown in Figure 4.2. Although the aim was to generate data points between 0% and 100%, it was not possible to obtain sand samples with relative densities between 82% and 100%, because the compaction could not be adequately and sensibly controlled within this region in spite of many trials. The main challenge was attributed to the smaller range of index unit weight values (from 16.4 kN/m^3 to 17kN/m^3) in high relative density (82% to 100%). Similar was case for relative densities (D_r) less than 50%.

The minimum index unit weight and respective resistance values were not included in the plot (Figure 4.2) due to the substantial gap between D_r = 0% and D_r = 50%, which would create an unrealistic estimation of relative densities lower than 50%. Furthermore, the correlation for D_r lower than 50% is not practically useful as most sand embankments were compacted D_r well above 50%. After measuring the penetration resistance of a compacted sand embankment in the flume experiment, Figure 4.2Figure 4. was used to determine the relative density of the sand.

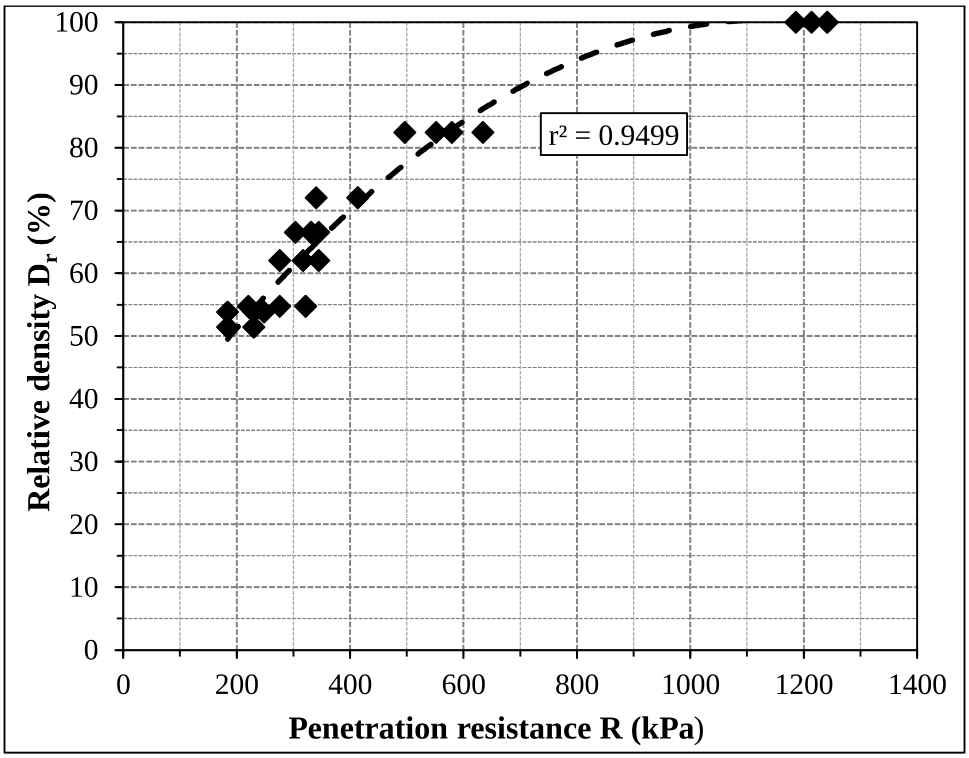

Figure 4.2 The correlation between penetration resistance and relative density of sand

4.2.4 Direct shear test

Direct shear tests of uniform sand (SP) were performed at a range of relative densities in the laboratory to obtain the respective shear strength of the compacted sand. To achieve target relative densities of 50%, 60%, and 80%, the masses of sand required were calculated and compacted in a shear box using a surcharge as shown in Figure 4.3. The difference in mass of shear box with and without compacted sand provided a check for actual mass of sand in the box. A detail calculation sheet was provided in Chakradhar (2014) – Appendix A.

The tests were performed at normal stresses ranging from 15kPa to 125kPa. A nonlinear (Figure 4.4) failure envelope was observed due to compaction of sand inside the shear box. The compaction caused interlocking and dilation of sand particles while shearing. A uniformly compacted sand layer couldn't be produced for $D_r = 50\%$ due to the greater effect of compactive force on top layer to lying underneath. It resulted in scattered points as shown in Figure 4.4. The compaction in thin layers for $D_r = 80\%$ produced more consistent results than in thick layers for $D_r = 50\%$. Therefore, a total of seven direct shear tests were carried out and an average curve was generated for $D_r = 50\%$.

a)

b)

Figure 4.3 The sand sample preparation for the direct shear: (a) compaction in shear box using surcharge; and, (b) sand sample after compaction

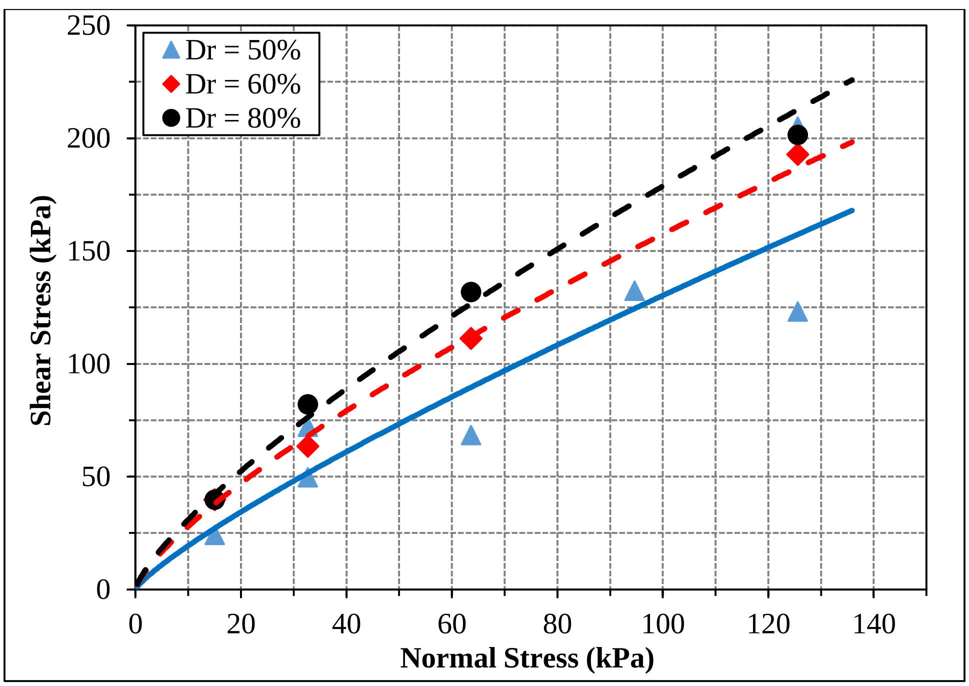

Figure 4.4 Mohr-Coulomb envelope for $D_r = 50\%$, 60%, and 80%

Using the failure envelopes developed in Figure 4.4 and the effective normal stresses calculated in Table 4.1 based on an 8-in (200 mm) thick model sand abutment with a water level at 5.5 in (140 mm), shear strengths (τ) of model soil were determined and plotted with their corresponding relative densities in Figure 4.5.

Table 4.1 Stresses of sand at three different relative densities

Relative Density, D_r (%)	Unit Weight, γ (kN/m^3)	Normal Stress at 8-in Depth, σ (kPa)	Pore Pressure of 5.5-in Water, u_w (kPa)	Effective Normal Stress at 8-in Depth, σ' (kPa)
50	15.4	3.05	1.36	1.69
60	15.7	3.11	1.36	1.75
80	16.4	3.25	1.36	1.89

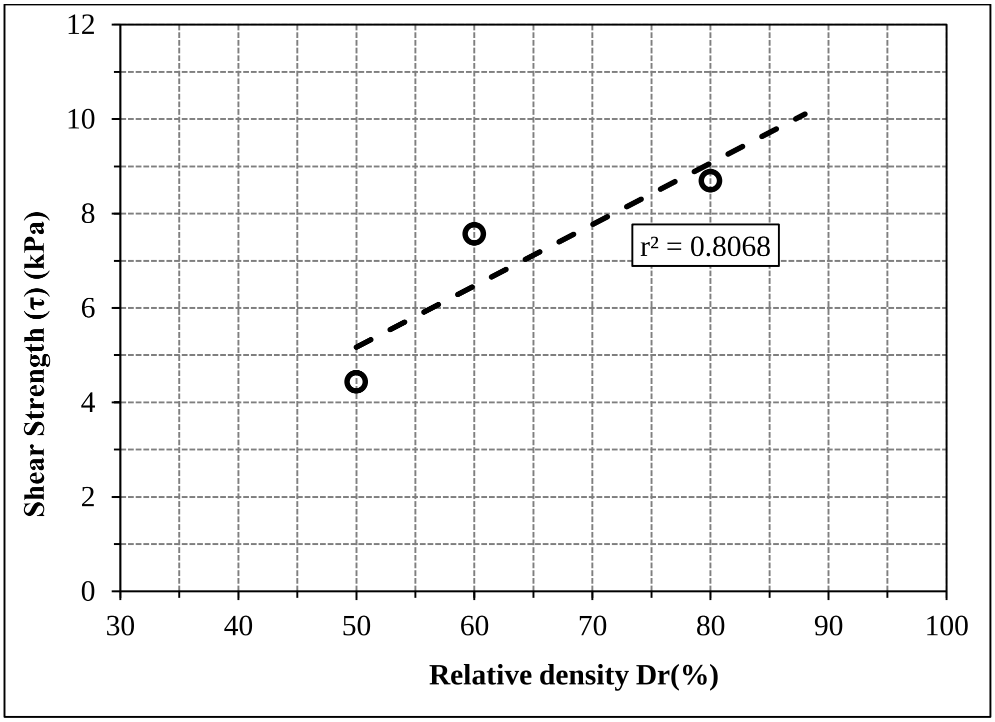

Figure 4.5 A relationship of shear strength and relative density of sand

4.3 Tests on Cohesive Soil

Samples of cohesive soil were collected from a site at the University of Wyoming as shown in Figure 4.6. The principle engineering properties of this soil were particle size distribution, Atterberg limits, maximum dry density, optimum moisture content, and shear strength.

The following laboratory tests were conducted to determine the engineering properties of cohesive soil:

I. Particle size distribution
   a. Sieve analysis
   b. Hydrometer analysis
II. Atterberg limit test
   a. Liquid limit test
   b. Plastic limit test
III. Standard Proctor test

IV. Direct shear test, and
V. Undrained shear strength test using a hand-held pocket penetrometer and a torsional vane shear device

a) b)

Figure 4.6 a) The soil source used to obtain the cohesive soil for this study and b) sample quantities of cohesive soil collected for this study

4.3.1 Particle size distribution

An air dried sample was prepared in accordance to the soil testing standard ASTM D421-85, and the sieve analysis and hydrometer analysis were carried out as per the standard ASTM D422-63. A stack of ASTM standard sieves shown in Figure 4.7 was used for the sieve analysis. ASTM 151h hydrometer confirming the requirement stated in ASTM specifications E100 was used for the hydrometer analysis (Figure 4.8). A sample detail calculation sheet used in determining particle size distribution was summarized in Chakradhar (2014) – Appendix B. The data obtained from the sieve and hydrometer analyses were used to construct the particle size distribution curve presented in Figure 4.9.

Figure 4.7 Set up for the sieve analysis tests

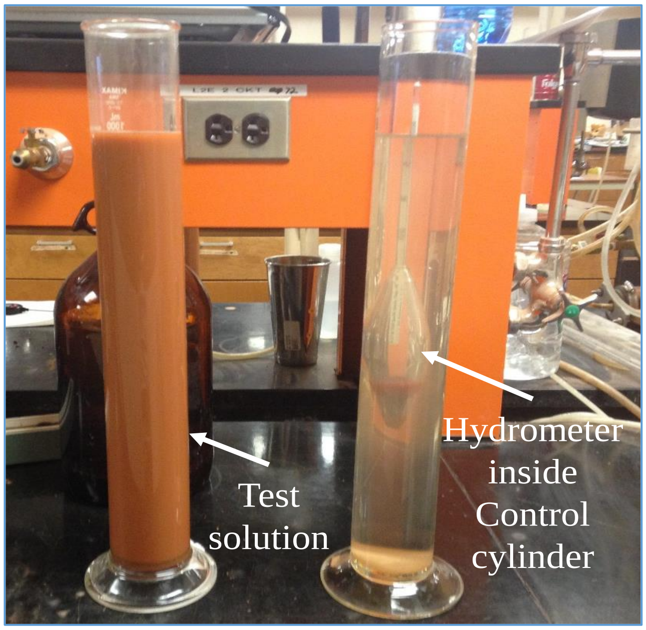

Figure 4.8 Set up for the hydrometer analysis

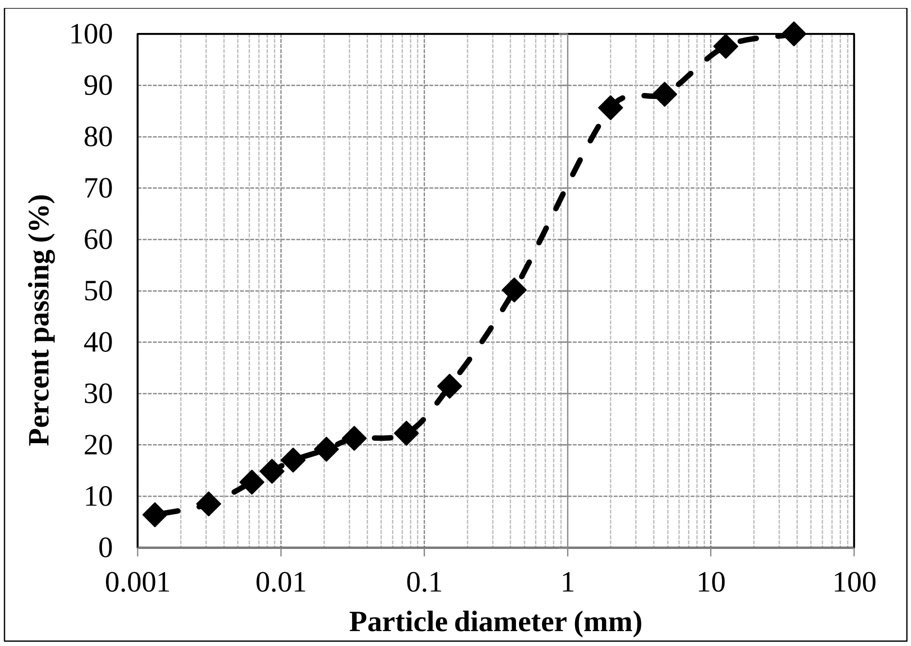

Figure 4.9 Particle size distribution curve for the cohesive soil

4.3.2 Atterberg limit test

The Atterberg limit test includes the determination of the Plastic Limit (PL), Liquid Limit (LL), and Plasticity Index (PI) of cohesive soil and was conducted in accordance with the ASTM standard test procedure D4318-10. Atterberg limits are defined in terms of moisture content. The Liquid Limit (LL) is moisture content when the soil changes from a plastic to a viscous fluid state. Equipment used for the test is shown in Figure 4.10. The liquid limit of the cohesive soil used for the study was 22.5% (≈ 23%) as shown in Figure 4.11.

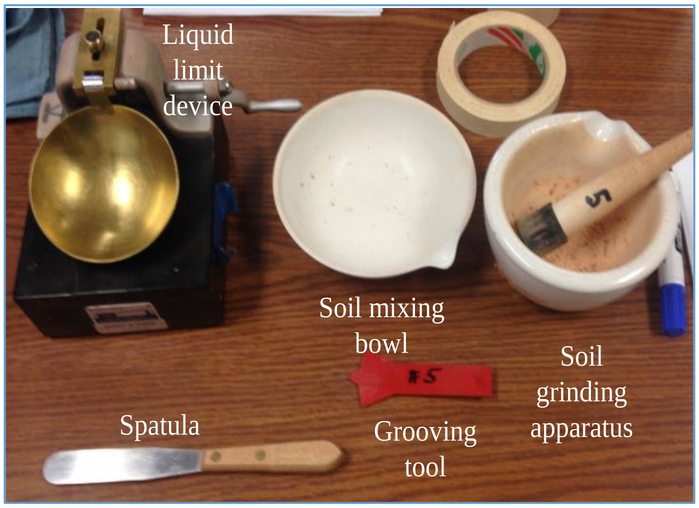

Figure 4.10 Equipment used for the liquid limit test

The moisture content at which the soil changes from semi-solid to plastic is the Plastic Limit (PL). It is the water content at which soil begins to crumble when rolled into 3 mm (1/8-in) in diameter as shown in Figure 4.12.

The Plasticity Index is the range of water content over which soil remains plastic. Numerically, it is a difference between LL and PL; i.e.,

$$PI = LL - PL \tag{0.1}$$

A sample calculation for tests on cohesive soil was shown in Chakradhar (2014) – Appendix B. Based on the measured PL of 16% and LL of 23%, the Plasticity Index of the soil was determined to be 7%, which indicated the soil is less plastic.

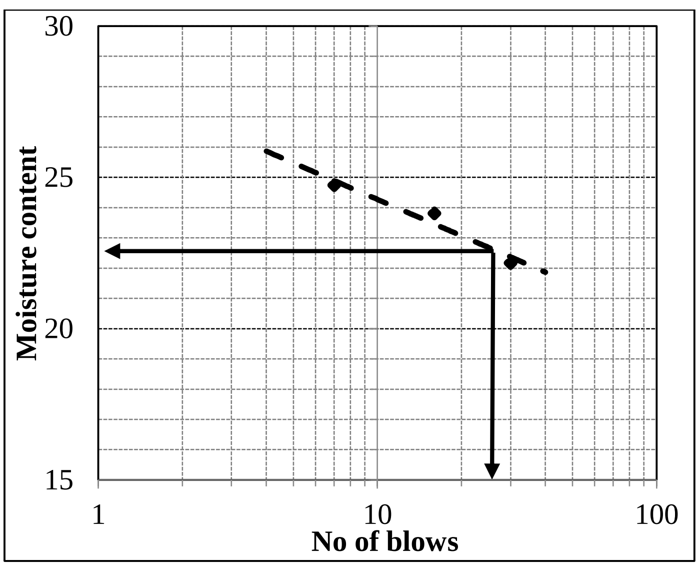

Figure 4.11 Liquid limit graph

Figure 4.12 Plastic limit test with a rolled sample of cohesive soil

4.3.3 Soil classification per the Unified Soil Classification System (USCS)

Soil type is classified using the Unified Soil Classification System (USCS) as per ASTM D2487. The particle size distribution showed that the soil has only 22% fines, and more than 50% of the particles passed through sieve No. 4, which indicates that the soil has more sand material. Based on the measured LL of 23% and PI of 7%, the soil lies above the “A” line in the plasticity chart shown in Figure 4.13. Hence, the soil is classified as Clayey Sand (SC) as per USCS.

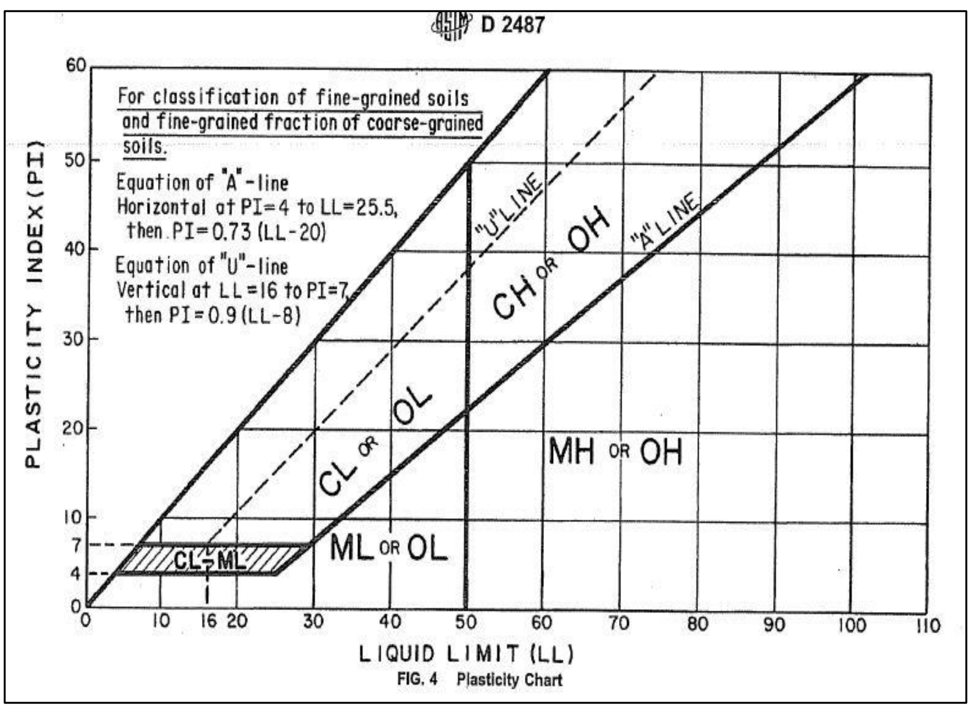

Figure 4.13 Plasticity Chart taken from the ASTM D2487

4.3.4 Standard Proctor test (compaction test)

The standard Proctor test is a laboratory compaction test for cohesive soil. In this test, soil at different moisture content is compacted in a 101 mm (4 in) Proctor mold with a standard 24.4N (5.5 lbf) rammer dropped from a height of 305 mm (12 in). The standard test procedure, as illustrated in Figure 4.14Figure 4.14, was carried out in the laboratory in accordance with ASTM D 698-91. Plotting dry unit weights with the respective moisture contents gives a compaction curve shown in Figure 4.15. This curve was used to determine the maximum dry unit weight or dry density (MDD) from the moisture content of soil.

Figure 4.14 Soil-water mix (left top), soil compacted slightly above top collar (right) and soil after compaction (bottom left)

The maximum dry unit weight was 19.45kN/m^3 (123 pcf) and the corresponding optimum moisture content was 12%. The deatiled calculation was summarized in Chakradhar (2014) – Appendix B.

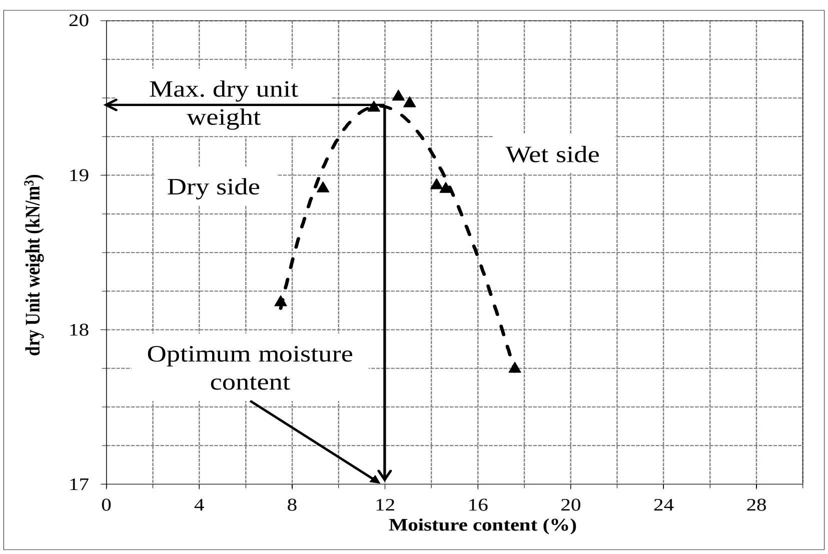

Figure 4.15 Compaction curve determined using the standard Proctor test

After completing the standard Proctor test, a hand-held penetrometer and a torsional vane shear device were used on the same compacted soil as illustrated in Figure 4.16, Figure 4.17, and Figure 4.18, respectively, to determine the undrained shear strength (S_u). A minimum of four tests were performed on each soil sample compacted ranging from 89% to 100% of maximum dry unit weight. At compaction below 89% (wet side), the moisture content was high, which increased the adhesion of soil to the proctor hammer and thereby hindered compaction. At dry side (Figure 4.15), tests using hand held devices couldn't be performed due to the difficulty in obtaining an adequate penetration. Hence the test was carried out only on the wet side of compaction. The relevant calculations were included in Chakradhar (2014) – Appendix B. The measured undrained shear strength of a series of carefully compacted moisture controlled soil samples were used to generate the plots shown in Figure 4.19, Figure 4.20, and Figure 4.21.

The results showed that the torsional vane shear device produced a consistent and excellent correlation ($r^2 = 0.95$) compared with the pocket penetrometer ($r^2 = 0.81$). It was also observed that the undrained shear strength determined using a pocket penetrometer was always higher than that obtained using the torsional vane shear device. The main reason leading to this outcome was the ability of the shear device to measure the shear strength as small as 0.05kg/cm^2 with a permissible visual interpretation to the nearest 0.01kg/cm^2 while the pocket penetrometer gives the reading with an accuracy of only 0.125kg/cm^2. Therefore, the torsional vane shear device was adopted in the subsequent flume experiments. During the experiments, the percent compaction of a clayey sand embankment was estimated based on the measured undrained shear strength (S_u) using the torsional vane shear device and the correlation given in Figure 4.21.

Figure 4.16 A pocket penetrometer test performed on a soil sample compacted using standard Proctor method

Figure 4.17 A torsional vane shear test performed on a soil sample compacted using standard Proctor method

Figure 4.18 A soil sample after completing five torsional vane shear and four penetrometer tests

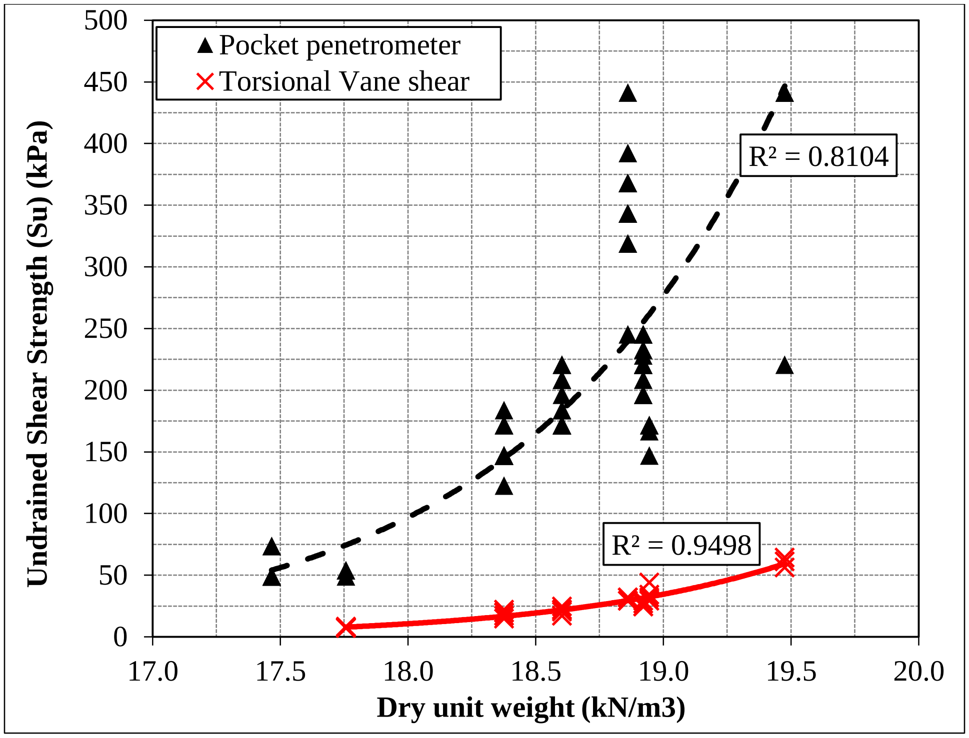

Figure 4.19 A plot of dry unit weight vs. undrained shear strength of clayey sand

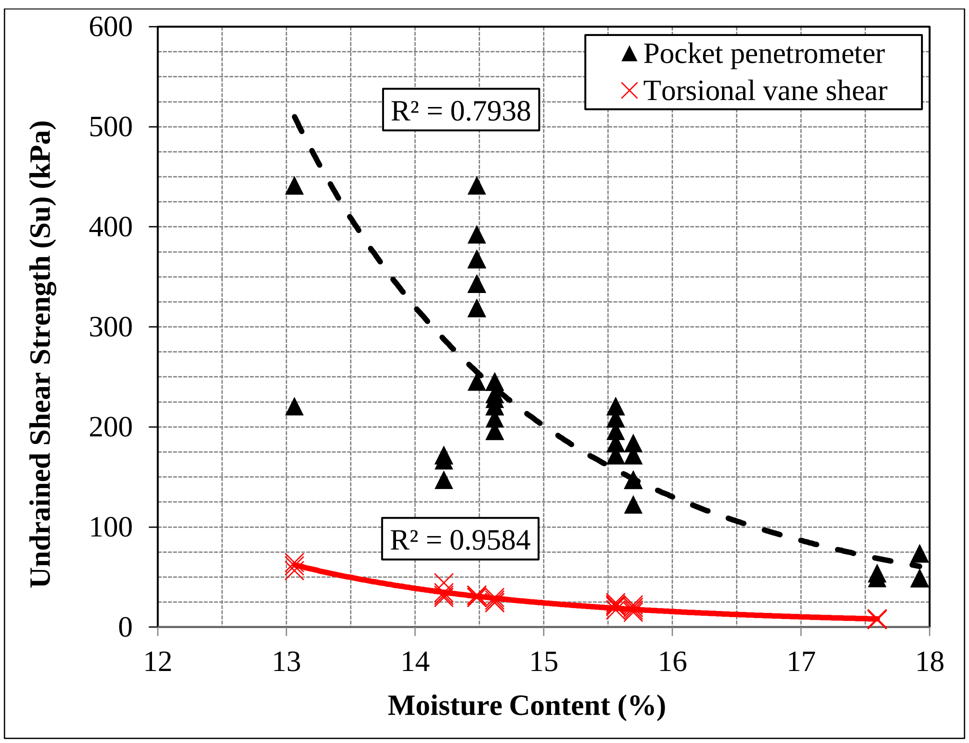

Figure 4.20 A plot of moisture content vs. undrained shear strength of clayey sand

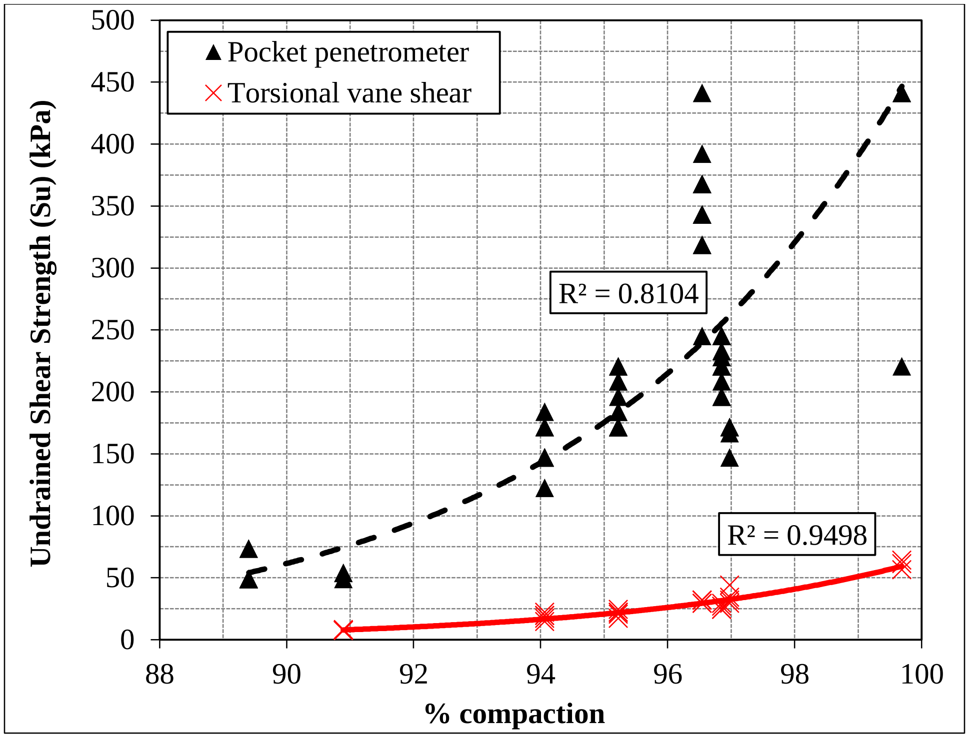

Figure 4.21 A plot of percent compaction vs. undrained shear strength of clayey sand

4.3.5 Direct shear test (DST)

Shear strength is an important engineering property of soil used to determine the stability of slopes or cuts, bearing capacity of foundation, and lateral earth pressure on retaining structures. Accordingly, it is important for assessing the stability of abutment spill-slopes subjecting to scour. Soil shear strength is attributable to inter-particle interactions that act to resist shear stress applied to the soil. The two components contributing to soil shear strength are cohesion (c) and friction angle (ϕ). Direct shear test was performed in the laboratory to determine the shear strength of clayey sand in accordance with ASTM D 3080. Figure 4.22 shows the setup of a direct shear test.

Three clayey sand samples at 91%, 97%, and 98% of maximum unit weight (or MDD) were prepared using the standard Proctor method as described in Section 0 4.3.4Standard Proctor test (compaction test). A 63.5 mm (2.5 in) diameter Shelby tube with a metal plate (Figure 4.23) was custom-made to collect a 63.5 mm (2.5 in) diameter undisturbed soil sample pushed from the 101.6 mm (4 in) Proctor mold using a soil extruder as shown in Figure 4.23 and Figure 4.24. The process of sampling the soil into the Shelby tube was carried out with caution to minimize soil disturbance and maintain the moisture. The greatest challenge was to trim a soil sample into a 25.4 mm (1 in) in length without crumbling the soil, especially a drier soil, as illustrated in Figure 4.25Figure. Another challenge was to obtain a completely smooth cut surface, which was required to distribute a normal stress uniformly.

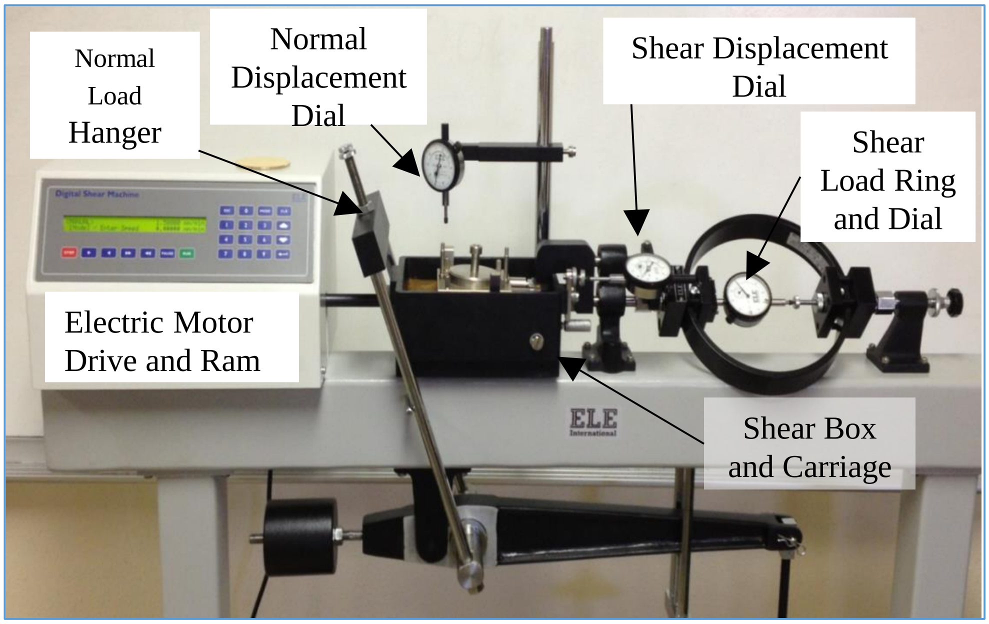

Figure 4.22 Direct shear test setup

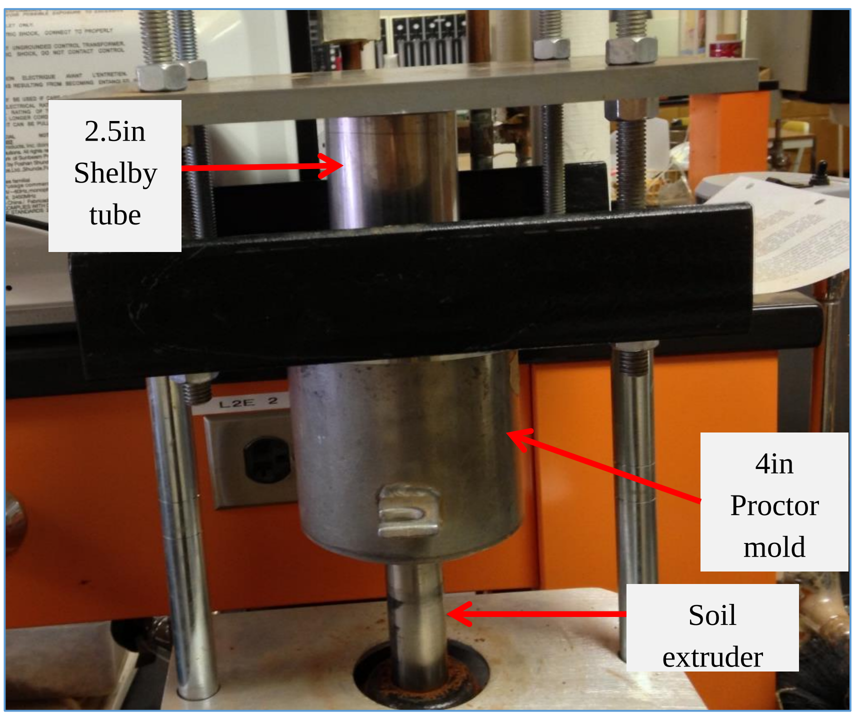

Figure 4.23 Test arrangement for extracting a soil sample from a standard Proctor mold into a Shelby tube

Figure 4.24 Illustrations showing how a soil sample was extracted into the Shelby tube

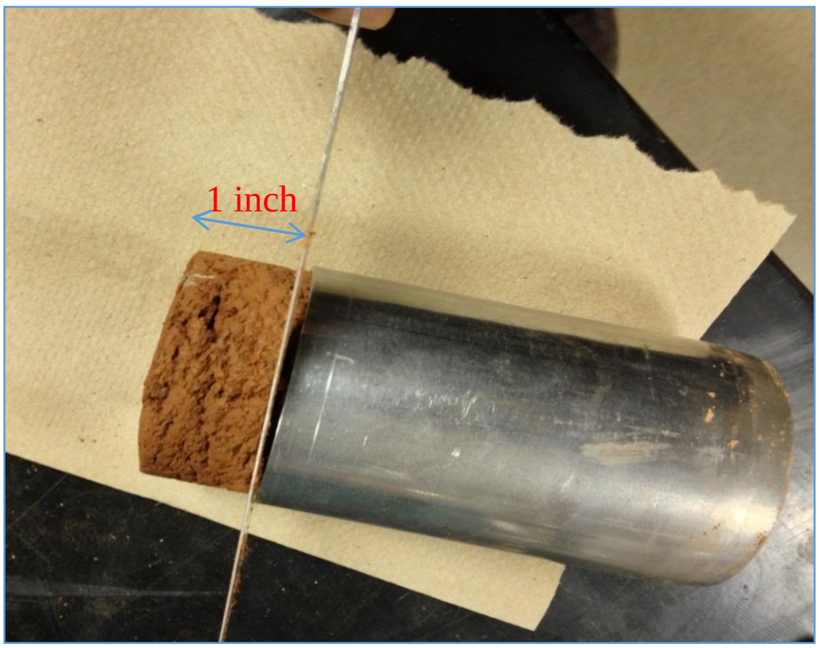

Figure 4.25 Trimming the soil cut to 25 mm (1 in.) for use in the direct shear test

The three ultimate shear stresses of each SC soil discussed above are plotted against the respective normal stresses applied during direct shear test to develop a Mohr-Coulomb failure envelope as shown in Figure 4.26. The failure envelopes are straight line, whose slopes being friction angle and the y-intercept cohesion.

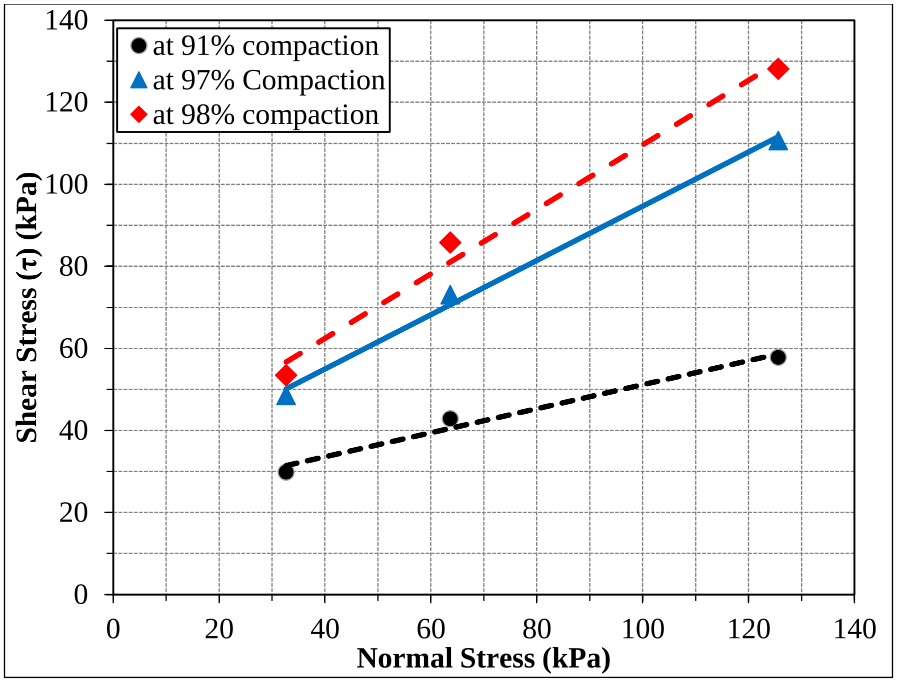

Figure 4.26 A plot of normal stress vs. shear stress of clayey sand obtained from direct shear tests

The cohesion and friction angle of the SC soil obtained from the direct shear test as well as other shear strength properties are summarized in Table 4.2. The shear strength (τ) was calculated using the linear Mohr-Coulomb relationship,

$$\tau = c + \sigma \times \tan(\phi) \quad (0.2)$$

where,
τ = shear strength of soil,
c = the cohesion,
σ = the normal stress applied on soil, and
ϕ = is the friction angle.

Table 4.2 Soil properties at three levels of compaction

Percent Compaction, %	Unit weight, γ, (kN/m^3)	Cohesion, c (kPa)	Friction Angle ϕ (deg.)	Normal Stress at 200mm depth σ_v, (kPa)	Shear Strength, τ (kPa)
91	17.71	21.86	16.3	3.51	22.89
97	18.87	28.59	33.4	3.75	31.06
98	19.07	28.45	39.0	3.79	31.52

Note: h = height of model embankment soil used in flume experiments = 200 mm (7.87 in)

Plotting the percent compaction against the estimated shear strength summarized in Table 4.2, a correlation was developed in FigureFigure 4.27 to determine the shear strength of SC soil compacted at any percent compactions above 90%.

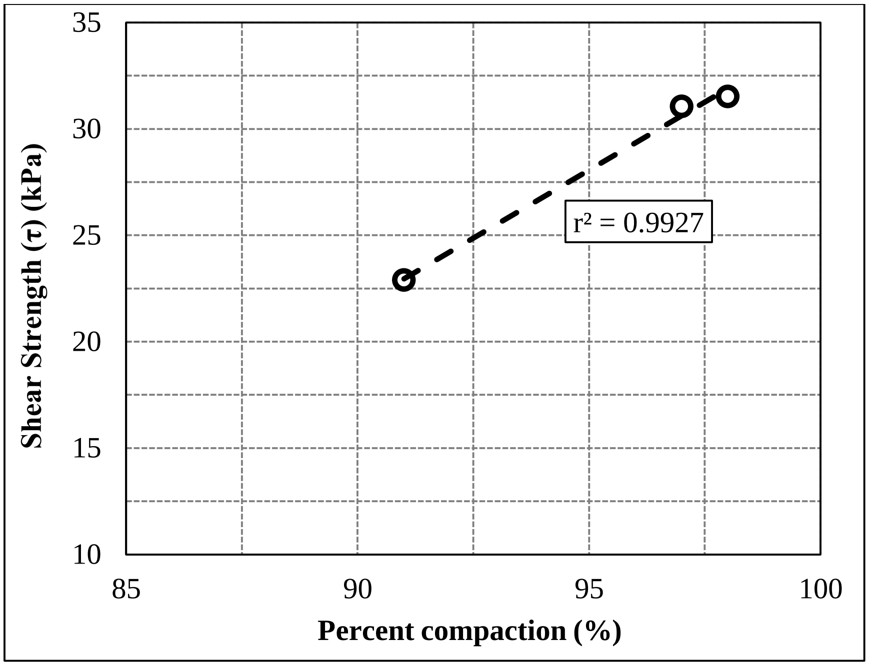

Figure 4.27 Plot of percent-compaction vs. shear strength of the cohesive soil

4.4 Tests on Sand Clay Mix Soil

Two flume experiments were conducted using sand clay mix to cover a range of soil types. The mix was prepared using 80% of uniform sand and 20% of clay content from clayey sand. The main objective was to generate soil type having shear strength in between uniform sand and clayey sand. Therefore, no detail laboratory soil tests were performed. The engineering properties investigated were

- unit weight by compaction
- penetration resistance using needle penetrometer
- shear strength by direct shear test

4.4.1 Determination of unit weight and penetration resistance

The two mix soil samples with different unit weights were prepared in a mold with an inside diameter of 152.4 mm (6 in), and height equal to 114 mm (4.5 in). A Proctor hammer was used for compaction to achieve the respective unit weights. The unit weights were calculated using the weight of soil sample in the mold and volume of mold. The sample calculation was attached in Chakradhar (2014) – Appendix C. Penetration resistance for the sample so prepared were then determined using needle penetrometer. The two tested samples had unit weights 16kN/m^3 (R = 192 psi) and 15.7kN/m^3 (R = 145.5 psi). In-flume compaction measurements, by means of in-situ penetration resistance values, were performed to ensure these values of unit weight were attained.

4.4.2 Direct shear test

The sand-clay mix was compacted in a shear box to achieve dry unit weights 16kN/m^3 and 15.7kN/m^3 and loaded in a shear machine to perform a direct shear test. A Mohr-coulomb envelope was developed for the two soil samples as shown in Figure 4.28.

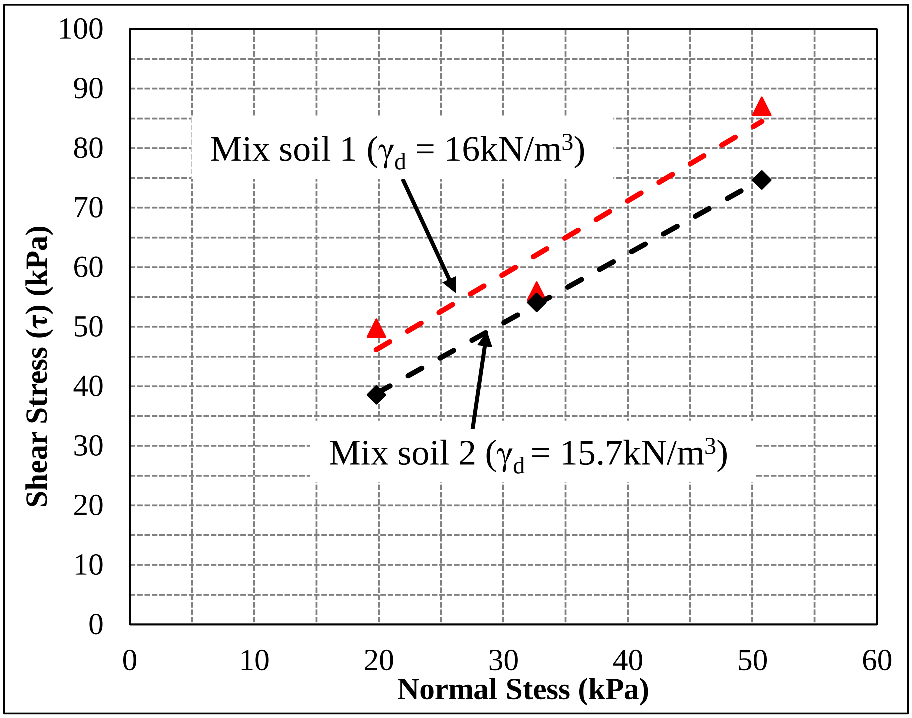

Figure 4.28 Mohr's Coulomb envelope for two mix soil samples having unit weights $16 kN/m^3$ and $15.7 kN/m^3$

The values of cohesion and friction angle were computed from the Mohr-Coulomb envelope, and are presented in Table 4.3. The effective shear strength was computed for the effective normal stress experience by the soil at the base of embankment model (h = 0.2 m).

Table 4.3 Soil properties at three levels of compaction

Unit weight, γ (kN/m^3)	Cohesion, c (kPa)	Friction Angle, ϕ (deg.)	Normal Stress at 200mm depth, σ_v (kPa)	effective normal stress, σ' (kPa)	Shear Strength, τ (kPa)
15.7	15.736	49.3	3.14	1.78	17.81
16.1	21.64	51.1	3.22	1.85	23.94

5. FLUME EXPERIMENTS

5.1 Introduction

This section describes the setup and procedure for conducting the flume experiments. The procedure included preparation of the flume, embankment model construction methods, the flow, instruments used and setup, sequence of experiments performed, and the subsequent data analyses. Table 5.1 is a summary table of the flume experiments performed.

5.2 Flume Overview

The experiments involved constructing a 1:30-scale model channel and abutment in the large flume situated in the Water Resource Laboratory at the University of Wyoming. The flume is an 18.29 m (60 ft) long and 3.66 m (12 ft) wide wooden channel as shown in Figure 5.1. The test section occupied an area of 2.44 m (8 ft) wide by 3.66 m (12 ft) long, as depicted in Figure 5.1. The experimental channel consisted of the test section and an upstream and a downstream section, both of which were formed using a raised plywood floor, 0.3 m (1 ft) above the flume. Figure 5.2 shows the setup of the flume, starting with placing the plywood to construct the approach and downstream sections, building a test section filled with sand, and forming the model abutment.

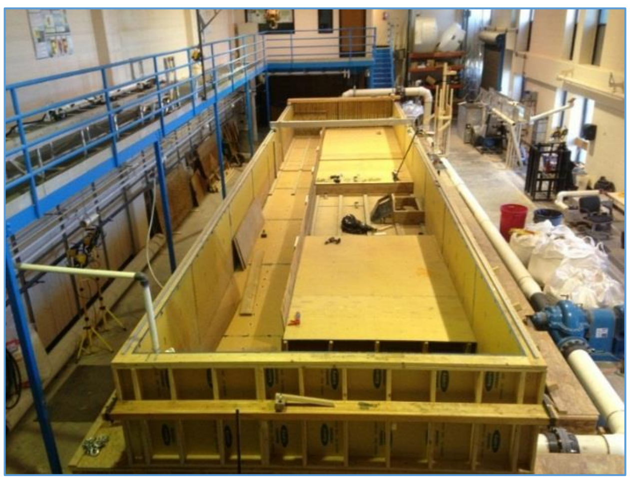

Figure 5.1 Overview of flume used for experiments

5.2.1 Flume and flow channel

The flume is composed of a head-box with a diffuser pipe, which discharged water from the recirculating pump as shown in Figure 5.3(a). A two-row wooden baffle rack shown in Figure 5.3(b) acted to spread the flow across the flume, and thereby established a more-or-less uniform distribution of flow entering the flume. Immediately after the water entered flow channel, it passed over a roughened bed section. It slowed the lower portion of flow so as to cause the flow to assume the vertical velocity profile associated with fully turbulent flow. This process occurs typically in open-channel flows. The bed roughness was formed by means of metal grit (about 1 mm diameter) glued to the flume bed.

Figure 5.2 Flume and test section setup: a) top left: vertical plywood to raise the floor, b) top right: false floor nailed on erected plywood with an empty test section, c) bottom left: uniform sand layer compacted using tapper, and d) bottom right: sand layer compacted to be flushed with false floor experimental setup

a) b)

Figure 5.3 Flow entry into the flume is guided by (a) diffusion pipe that discharges flow across the head-box; and (b) a wooden baffle-bar rack used to spread flow across the flume

Water flowed along the 2.44 m (8 ft) wide approach channel, formed by the plywood false floor, and then passed through the sand-bed test section fitted with the model abutment. It exited the test section and flowed over a downstream section formed by a plywood false floor, then discharged into a tail-box from where it was pumped back to the flume's head-box.

5.2.2 Sand bed and abutment

The test section was filled with clean, uniform, and medium-size sand; the same sand was used to form the model embankment. This sand was compacted to form a uniform horizontal sand bed 0.3 m (1 ft) deep, whose surface was flush with a plywood false floor. The total length of the abutment was 1.0 m (3.28 ft), and the model had a width of 0.6 m (2 ft) including 1V:1.5H side slopes. The abutment stood to a height of 0.2 m (0.66 ft) above the sand bed. The height of the abutment on the left part at front section was reduced by 50 mm, as shown in Figure 5.5, so as to provide a consistent benchmark for stopping each experiment. Once the embankment soil had eroded to expose this benchmark, the experiment ended. A detailed construction drawing of the abutment is shown in Figure 5.5.

The overall dimensions of the abutment are presented in Figure 5.4 and a three-dimensional sketch (Figure 5.6) can be referred to for a detailed view. The spill-slope of the embankment model had a top width of 0.4 m and a 1V:1.5H side slope on either side. As mentioned in Section 4, the erodible spill-slope and front portion of the model abutment were formed using sand, with some additional tests using clayey sand and clay-sand mix as the model soil. A fully rigid, non-erodible abutment was simulated using a metal form placed neatly over the abutment structure.

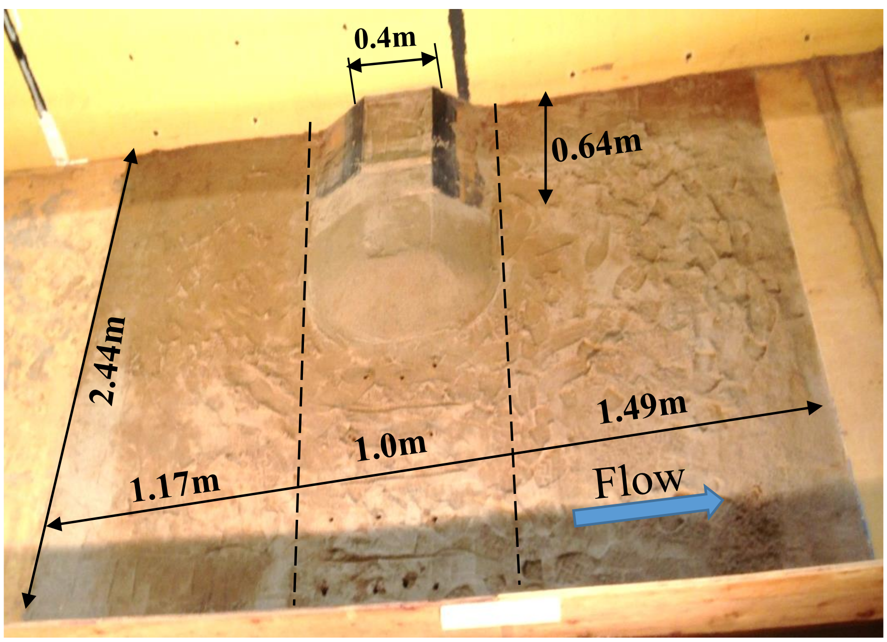

Figure 5.4 Dimensions of test section of flume experiments

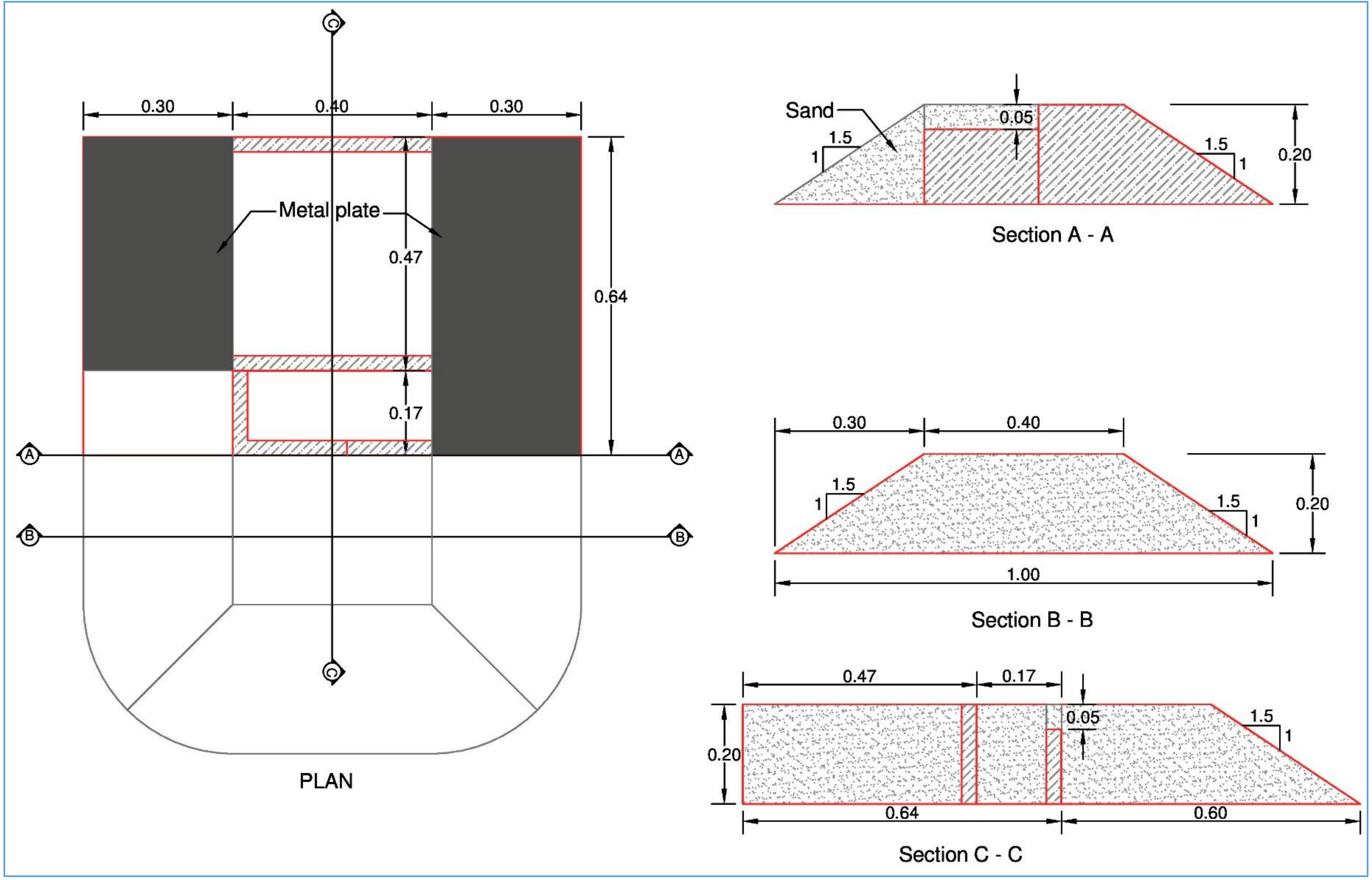

Figure 5.5 A Detail construction drawing of abutment (dimensions in meters)

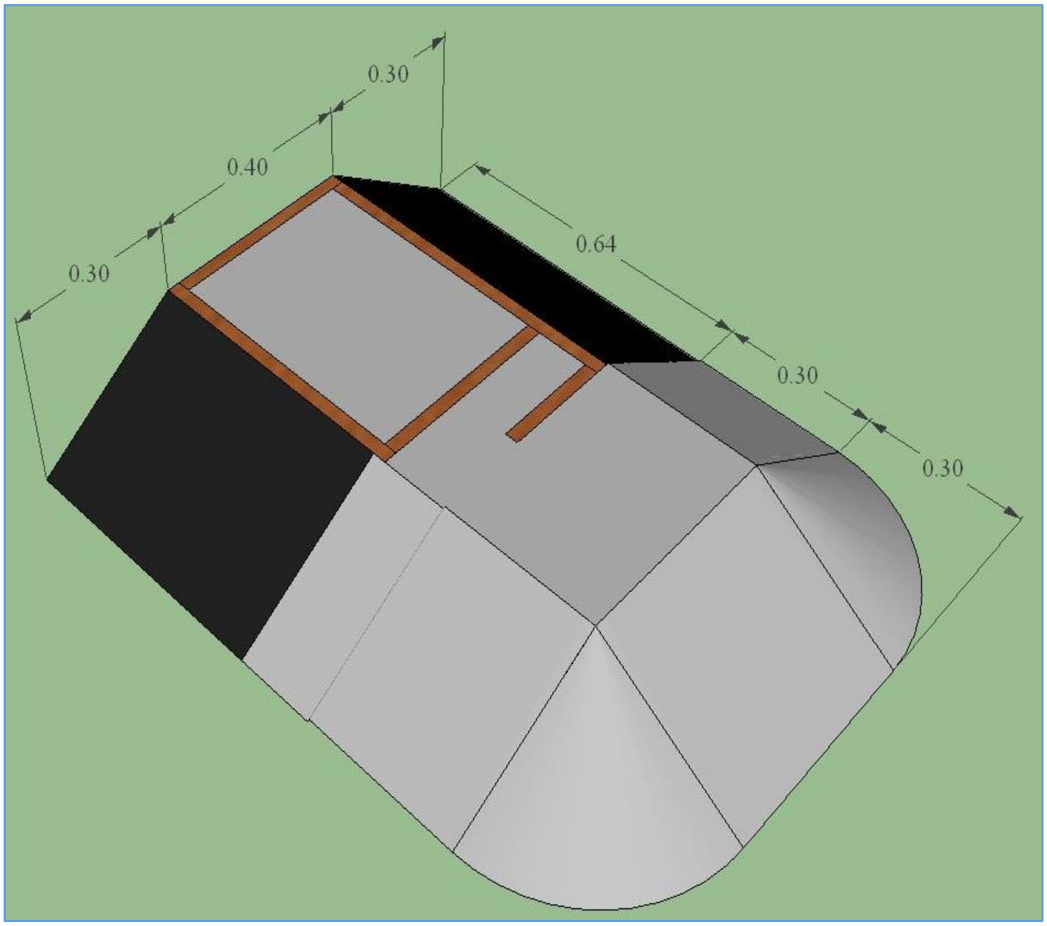

Figure 5.6 A three-dimensional sketch of erodible spill-slope of model abutment

The following procedure was followed to build the model spill-though abutments in the flume:

a) Embankment formed of uniform sand:

The uniform sand used for constructing the abutment spill-slope was mixed with water to make it wet and enhance compaction. The water for the mix was added to produce a moisture content equal to 10%, which was found (after a number of trials) necessary to ease compaction. Then a uniformly compacted sand bed base was prepared at the spill-slope base. A mark on the sand bed indicating the area to be covered by the spill-slope was made, and then the model sand was spread in layers. The sand was compacted in successive layers as shown in Figure 5.7, using a 203 mm (8 in) by 203 mm (8 in) and 4.65 kg flat tamper as shown in Figure 5.8. When the layer thickness was about 100 mm, the sand was compacted around the slope edges so as to maintain a slope of 1V:1.5H. While compacting close to the edge of a layer, a support to the slope surface was provided using a rectangular flat plate trowel to prevent collapse due to lateral pressure and vibration. This support helped to maintain the side-slope and make it smooth. The blow count on each layer was not recorded, but greater care was taken for the consistent compaction in individual layers. The embankment model was left to settle, if any, for a day before the experiment was performed.

Penetration resistance was performed using the needle penetrometer and moisture content (via an oven dry method) was recorded before each flume experiment. These tests were performed on soil at the top of the embankment.

Figure 5.7 Pictures showing the layered compaction of sand abutment spill-slope

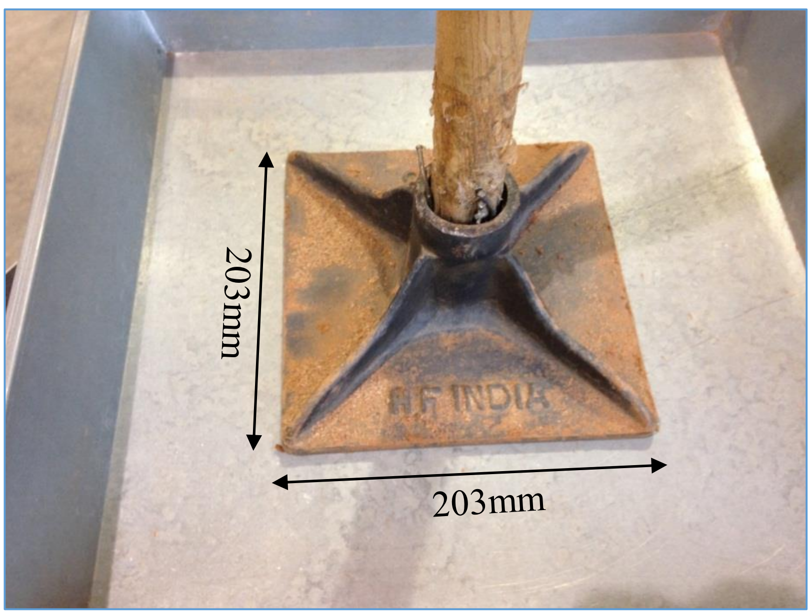

Figure 5.8 Tamper used to compact the layers of sand forming the model abutment

b) Embankment formed of clayey sand (SC):

A similar construction procedure as explained in a spill-slope formed of sand was followed for the spill-slopes formed of clayey sand. The target densities were achieved by mixing the soil with calculated moisture content and compaction. The mixture was prepared on the false floor before it was compacted in layers in the test section as shown in Figure 5.9. A manual procedure using hand shovels was used to prepare the mix. Spreading of soil, sprinkling water, and mixing were carried out carefully to produce a homogeneous mix. The compaction was carried out following the same procedure as for the spill-slope formed of sand.

Figure 5.9 Layered compaction of SC soil forming abutment spill-slope

A torsional vane shear tester was used to measure the undrained shear strength (S_u) as discussed in Section 4. Respective moisture content was also recorded.

c) Embankment formed of sand clay mix:

Mix soil was prepared by mixing 80% sand and 20% clay with water to prepare a consistent mix. The embankment formed of mix soil is shown in Figure 5.10. The procedure for spill-through abutment using sand was followed for mix soil.

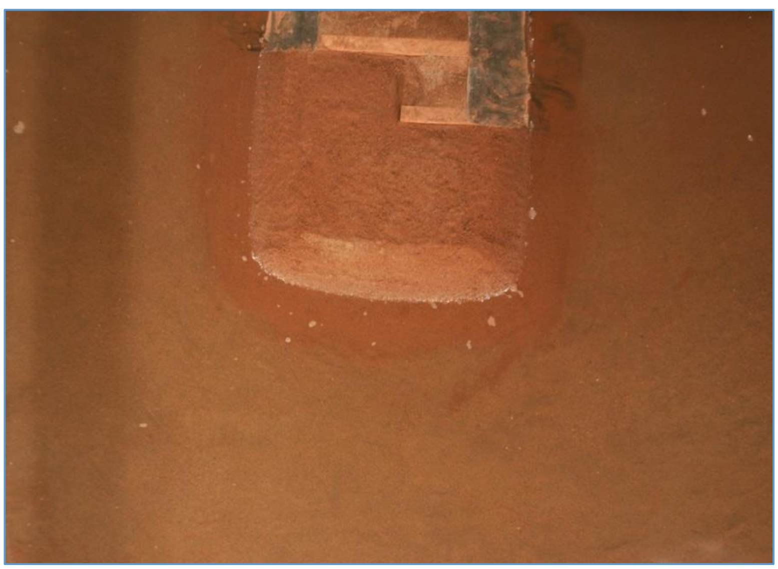

Figure 5.10 Embankment formed of mix soil with the flume filled with water

d) Spill-slope using non-erodible metallic plate:
A metallic (aluminum) plate was used to form a non-erodible spill-through abutment as shown in Figure 5.11. The metal plate spill-slope has the same dimensions as shown in Figure 5.5. The hollow space in the metal plate was filled with compacted soil to facilitate flow around the spill-slope rather than through it. Care was taken to stop the seepage of water from base and sides. The outer surface was protected using stone rip-rap at the thickness of 200 mm (8 in.).

Figure 5.11 Non-erodible (metal plate) with rip-rap surrounding the spill-slope to obtain maximum scour depth

5.2.3 Recirculating pump

A variable frequency driven pump was used to recirculate flow through the flume. For each experiment, the flow was constant at a steady discharge of $0.105 m^3/s$ (3.7 cfs). This discharge was obtained by setting the electronic speed-control for the pump's motor to a frequency of 34.1 Hz. Figure 5.12 shows the pump and speed-control nit used in the study.

Figure 5.12 The pump and motor unit, with electronic speed control, used to recirculate flow through the flume

5.3 Instrumentation and Data Acquisition

This section describes the instruments and data-acquisition system used for the flume experiments. It includes a brief introduction regarding the purpose of the instruments used, instrument location in the flume, and the data-collection process.

5.3.1 Plot Stalker time-lapse Camera

A Moultrie Plot Stalker time-lapse 8.0 MP camera was used to take series of photographs from the side of the model abutment, and sometimes from above the model, so as to capture visual records of scour development. This camera has a programming feature to take time lapse photographs that facilitate in creating a record of progressive embankment failure with a time and date stamp on it. A time lapse of 10 seconds was set for all the experiments. For higher picture quality, the test section was illuminated using six halogen lights as shown in Figure 5.13; four placed at the front facing the embankment and two at the height targeting test section.

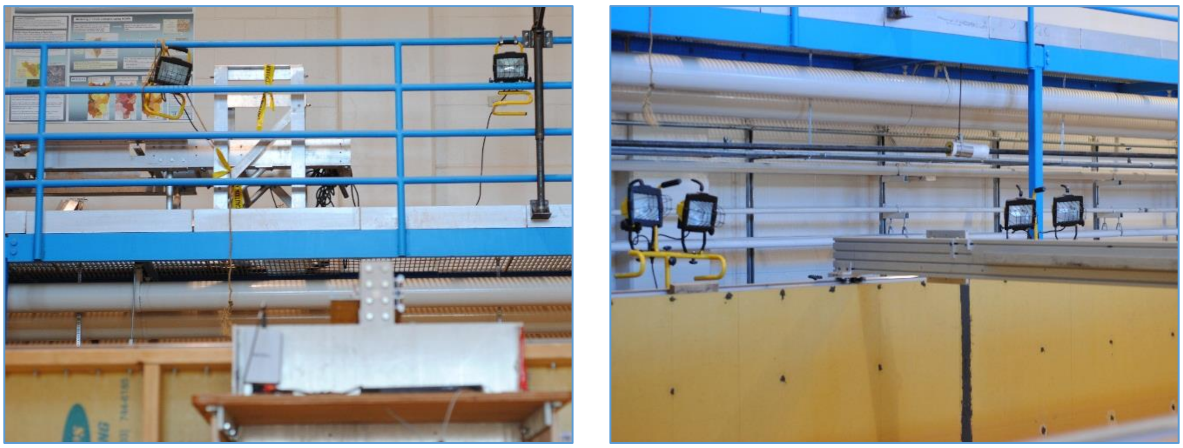

a) b)

Figure 5.13 Photographs showing halogen light setup a) at height targeting test section, and b) at the front facing abutment

5.3.1 Instrument beam with linear actuators

The flume's instrument beam, with the linear actuator and stepper motor attached, was used to automate the linear movement of the acoustic transducer that enabled the scour bathymetry to be recorded in real time. The acoustic transducer was attached to the movable carriage mounted on the beam as shown in Figure 5.14. The beam, built from high tensile aluminum, was fitted with an electromagnetic device called a stepper motor that achieves mechanical movement through the electric pulse. The stepper motor is used for the precise position control that followed a digital pulse sent from a laptop computer. It helped to change the relative position of a plate mounted on beam. A non-commercial executable, which recorded and saved the absolute position and respective time in a text file, was developed to control the movement

Position markings were placed on the beam to identify the positions defined in "carriage.exe" as shown in Figure 5.15. The position at X = 0 was assumed origin. The position at X = 0.61 m was set as the positive farthest position to which the carriage could travel. The position at X = -0.49 m, the location close to the front edge of the abutment spill-slope, was set as the back scan limit during experiments. Beside the locations where movement of the carriage was restricted by the abutment structure, a full scan of the cross section was performed up to X = -1.13 m.

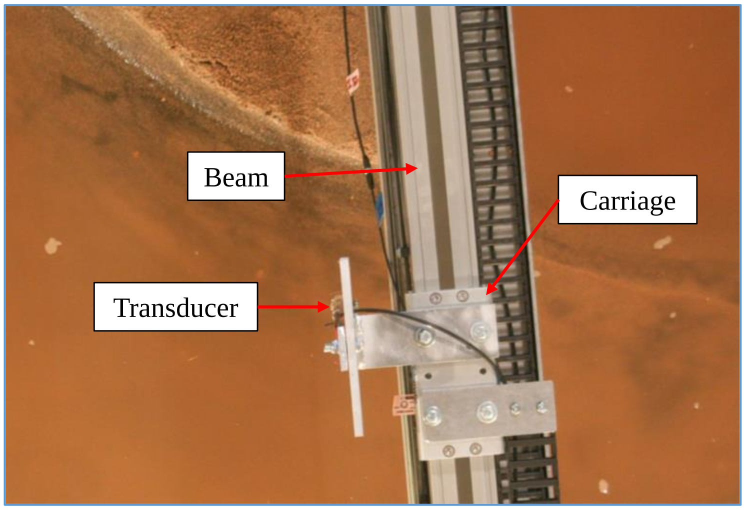

Figure 5.14 Movable carriage on beam

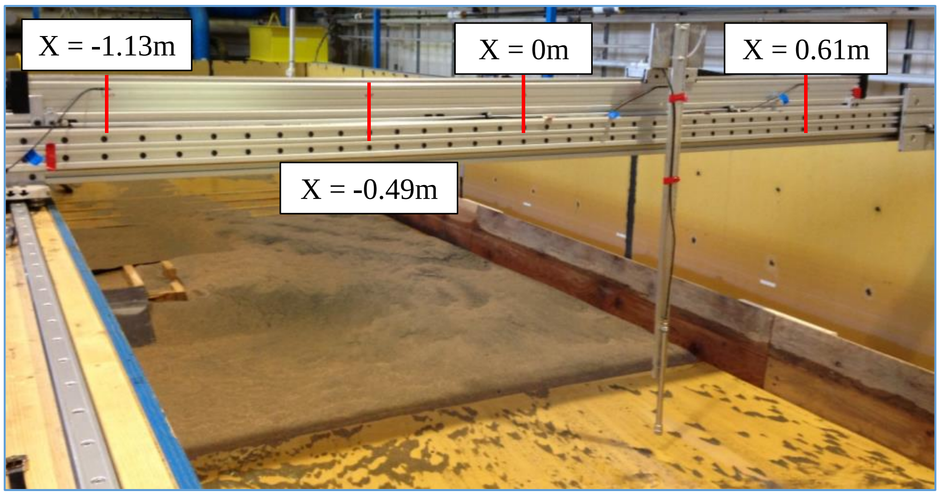

Figure 5.15 Position markers on beam

5.3.3 Ultrasonic acoustic transducer

a) Instrument

An ultrasonic acoustic transducer was used to measure scour depth in the flume experiments. This transducer was enclosed into a flat end cylindrical tube and connected to the data acquisition system through cable arrangements. The cylindrical tube was attached vertically to a plate which is mounted onto the beam and controlled by the stepper motor and linear actuators as shown in Figure 5.16. The tube was submerged into the water throughout the experiments.

An ultrasonic beam produced from the source diverges. The beam is narrow in the near field (indicated by N in Figure 5.17) and diverges at the far end. It is called beam spread. A correction is required to minimize the error due to beam spread. In flume experiments, the transverse distance travelled by the transducer was 25 mm (1 in.) per second, with a record rate of 75 (average) readings every second. This closely spaced measurement mitigated the possible measurement error attributable to spreading of the transducer’s beam.

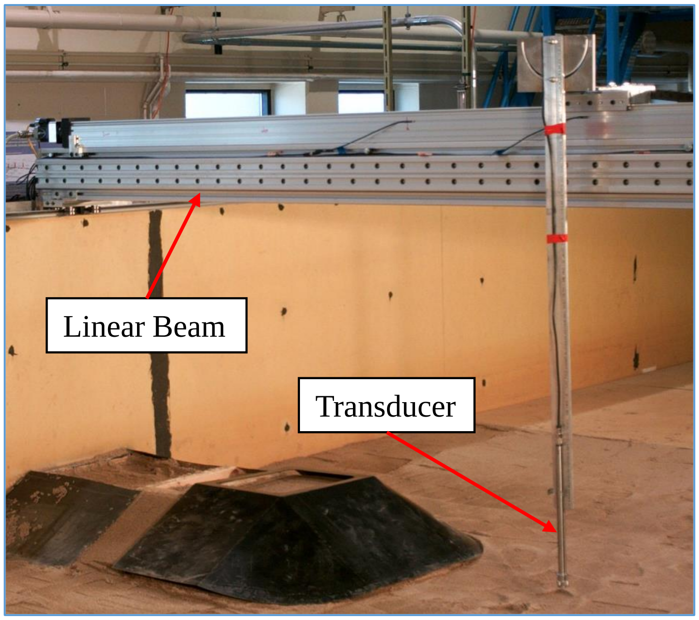

Figure 5.16 Instrument beam and transducer arrangement for scour depth measurement

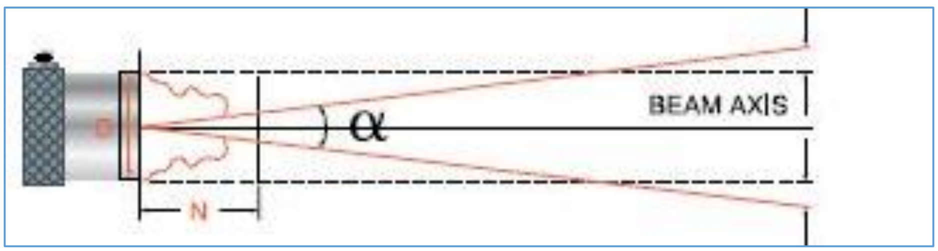

Figure 5.17 Beam spread emitted from transducer

b) Computation method

The ultrasonic sound produced from the transducer travels through the water and gets reflected back once it hits the soil surface. The time of sound wave propagation from the transducer, through water onto the sand and back to the receiver, is called time of flight (t). This real time record of time of flight is saved into a text file by an executable, which controls the transducer's ultrasound signal. Based on the velocity of sound wave in water (c = 1481 m/s at constant temp 20˚C) and time of flight, the distance from the transducer to the sand bed can be calculated using equation (5.1).

$$S = c \times \frac{t}{2} \tag{5.1}$$

where,
s = distance from transducer to sand bed,
c = velocity of sound in water at 20˚C, and
t = time of flight

The vertical distances computed using equation (5.1) are the relative distances of sand bed from the tip of transducer as shown in Figure 5.18. Similarly, the time versus position readings extracted from the carriage control executable generate absolute position X, Y, and Z as shown in Figure 5.18. The transducer, on average, records data at an interval of 0.1 sec and carriage position is recorded in every 10 milliseconds. It took 46 seconds to complete a full scan of total distance 1.1 m (from X = -0.49 m to X = 0.61 m). Hence, a linear interpolation is selected to compute the transducer reading at its absolute the position by a time series matching between the two output files. The error that could be generated using linear interpolation lies within a fraction of seconds, hence, could be negligible.

For the purpose of plotting position versus sand bed elevation, datum at a depth 1.00 m from the tip of transducer was established in order to get all the plots in a positive axis (first quadrant). As shown in Figure 5.18Figure , a, b, and c are the vertical distances calculated using the data produced from the transducer scan at each absolute locations (position X, Y, and Z). These values were subtracted from 1.00 m to obtain the respective sand bed elevation and plotted with respect to the transducer position.

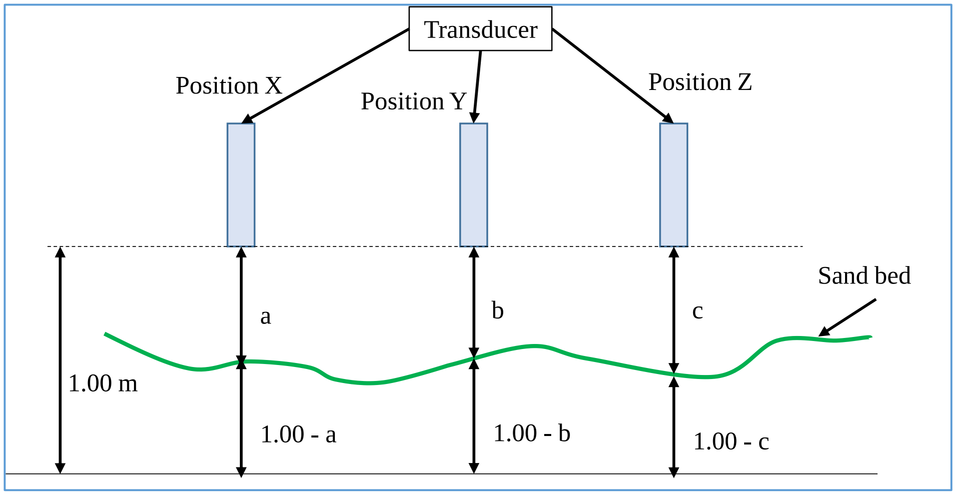

Figure 5.18 Depth of 1.00 m from Transducer tip used as datum for plot

5.3.4 Data acquisition system

A DPR500 Dual Pulser-Receiver, a modular instrument consisting of both pulser and receiver systems in one unit, was used as the data-acquisition system. It is designed to operate under a computer signal. The DPR500 produces a high voltage electrical excitation pulse on the remote pulser's ECHO connector with adjustable energy levels to adjust the strength of this excitation pulse. The ultrasonic transducer was connected to the ECHO connector via a short length of 50Ω coaxial cable. The transducer converts energy from the electrical excitation pulse into an ultrasonic pulse that propagates through water and gets reflected back. The acoustic echoes reflected from the sand bed would then be converted by the transducer into electrical signals to be processed by the DPR500 receiver. A detailed manual can be obtained from the following link (www.jsrultrasonics.com) or http://www.jsrultrasonics.com/documents/DPR500OpManual.pdf).

5.3.5 Beam- transducer combined application and data collection

The transducer's ultrasound signal was first stimulated by its executable using a computer before the movement of the carriage. Once it started recording data, executable controlling carriage movement was activated to trigger the linear actuator and initiate carriage movement. The center line of the abutment spill-slope model was selected as the scan path due to high constriction and, hence, being the most probable location for maximum scour depth. An initial scan of the sand bed after filling up the flume with water before running the experiments was carried out to obtain an initial bed profile. For the time series data collection, the movement of the beam's carriage-transducer arrangement was initiated immediately at the start of experiment, and start time was recorded.
The two output text files from executable programs that controlled the linear actuator and transducer provided (a) a useful time-series record of absolute position of the ultrasonic transducer across the flume

along the center line of abutment, and (b) the time-series record of total ultrasonic sound reflection. Hindsight showed that these two separate files could better have been combined as a single output, given the time and cost that would have been efficient and reduced the efforts on analysis.

5.4 Experiment Procedure

This section presents the procedure for running a flume experiment. The steps enumerated below were common for all experiments.

a) A compacted sand bed was prepared with uniform compaction throughout the test section; the sand bed was horizontal and flush with the false floor forming the approach bed and the downstream bed.
b) A homogeneous embankment soil-water mix was prepared and compacted on the sand bed to construct the embankment model following the steps discussed in Section 5.2.2. The compaction (and moisture content) was aimed to achieve target shear strength.
c) An indirect shear strength measurement of constructed embankment was performed using hand-held devices. A penetration resistance test using the needle penetrometer (Figure 5.19) was performed on the sand and mixed soil embankment models while a torsional vane shear test (Figure 5.21) was performed on clayey sand models. At least five in-situ strength tests at different locations on a finished surface of sand and mixed soil embankments were conducted, as shown in Figure 5.20 and Figure 5.23, to ensure compaction consistency. A number of torsional vane shear tests were performed on clayey sand as shown in Figure 5.22. The average value was used to correlate it to shear strength based on the correlation charts discussed in Section 4.
d) Additionally, penetration resistance tests using the needle penetrometer were performed on the sand bed along the transverse line of abutment to check its compaction consistency. At least three measurements were recorded in an interval of 30 cm (1 ft) from abutment spill-slope to the plywood wall as shown in Figure 5.24.
e) The instrumentation and data-acquisition systems were prepared and the transducer was aligned along the abutment's center line to collect sand bed scour profile data.
f) The flume was filled with water until 0.14 m (5.5 in) of the sand embankment was submerged leaving 60 mm of its total height exposed. The depth of water to be filled in the flume was determined from trial experiments and observations. The flow depth that was selected caused substantial scour, without the flow overtopping the abutment. The respective constant frequency of the recirculating pump was also set to achieve the flow depth.
g) Once the flume was filled, a sand bed scan was carried out to obtain an initial sand bed profile.
h) With the halogen lights on and a time lapse camera set to record mode, the recirculating pump was operated to initiate the experiment and the time of experiment was noted in the data sheet. Simultaneously, a bed scan using the acoustic transducer was carried out to collect real time scour depth data.
i) The pump operation was terminated once the abutment spill-slope was eroded and the wooden corner was exposed as shown in Figure 5.25 and Figure 5.26. The end time of the experiment was also noted in the data sheet.
j) Once water in the flume had come to a complete rest, a test section bathymetry data were collected starting at the upstream 1.40 m from the abutment center to 1.10 m downstream at an interval of 10 cm. This measurement of bed bathymetry provided scour profiles at different cross-sections.
k) When the scanning was completed, water was drained and the flume was left to dry for a day before next experiment was performed.

Figure 5.19 Penetration resistance test on a sand abutment spill-slope

Figure 5.20 Plan view of a sand abutment spill-slope with five penetration resistance tests

Figure 5.21 Torsional vane shear test on a clayey sand abutment model

Figure 5.22 Plan view of a clayey sand abutment model with 15 torsional vane shear tests

Figure 5.23 View of a sand-clay mix abutment spill-slope with five penetration resistance tests

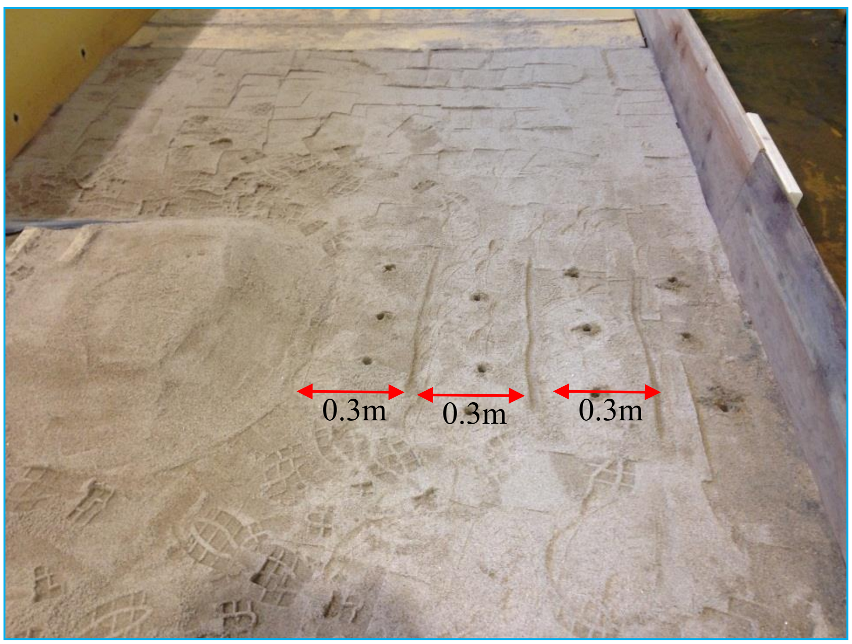

Figure 5.24 Penetration resistance tests on the sand bed at 30 cm (1 ft) intervals

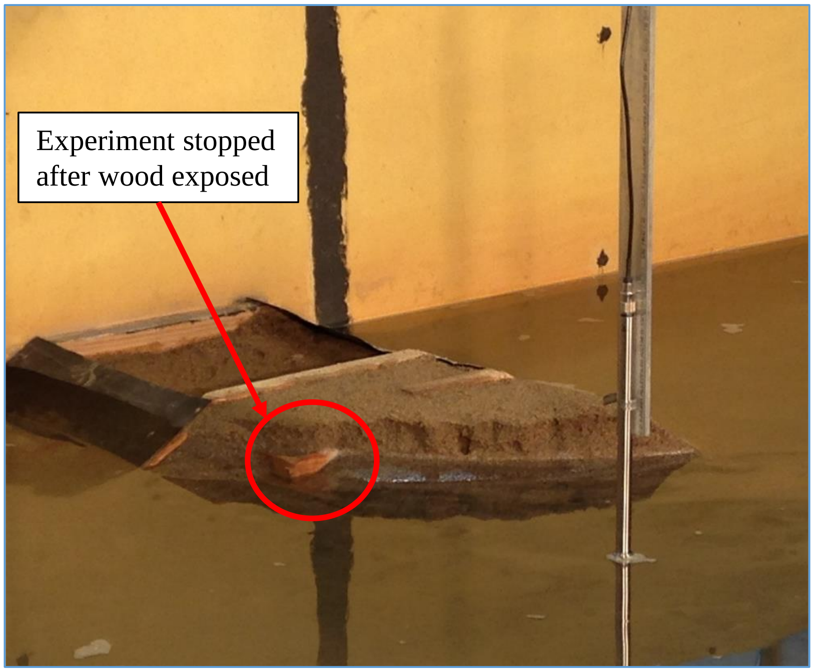

Figure 5.25 The benchmark indicating when to stop experiment

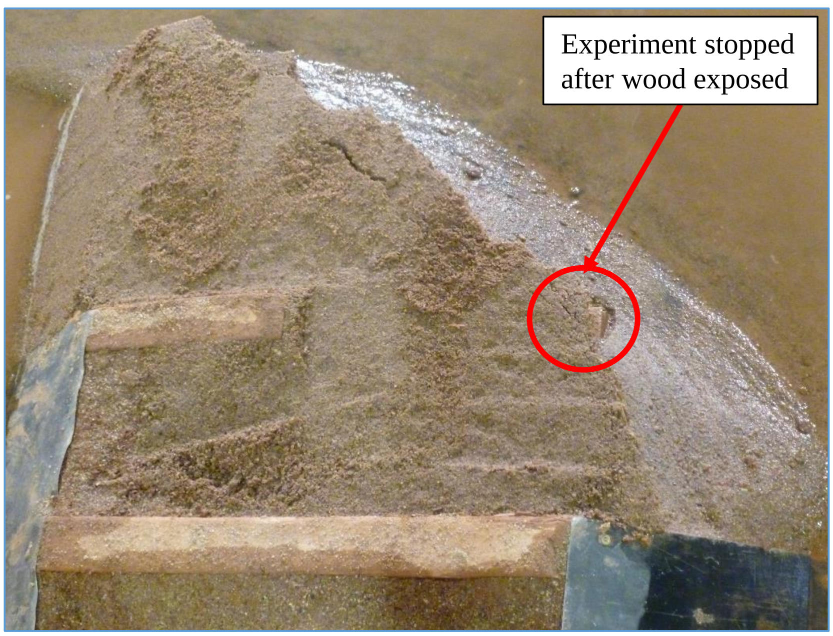

Figure 5.26 Plan view of indicator benchmark to stop experiment

5.5 Flume Experiment Summary

A total of 16 flume experiments were carried out following the procedure described in Section 5.4. The experiments consisted of eight experiments using sand embankment (S1 to S8), five using clayey sand (C1 to C5), two using sand clay mix soil (M1 and M2), and one experiment using a metal plate as a non-erodible embankment. Table 5.1 summarizes the flume experiments.

Table 5.1 Flume experiment summary

#	Experiment number	Abutment spill-slope soil type	Relative density/ percent compaction (%)	Abutment soil unit weight (kN/m^3)	Water content (%)	Shear strength (DST) (kPa)	Max. scour depth (cm)	Test time (hh:mm:ss)
1	S1	Sand	62	15.66	3.0	6.73	2.44	00:09:13
2	S2	Sand	74	16.06	3.60	8.28	2.89	00:08:26
3	S3	Sand	51	15.31	4.8	5.3	2.67	00:07:59
4	S4	Sand	83	16.38	3.4	9.45	3.63	00:10:46
5	S5	Sand	77	16.17	3.0	8.67	3.48	00:9:54
6	S6	Sand	75	16.10	2	8.41	3.26	00:08:44
7	S7	Sand	57	15.50	2	6.08	2.81	00:07:25
8	S8	Sand	70	15.93	3.0	7.76	2.67	00:08:25
9	R1	Rigid plate	-	-	-		10.14	00:50:24
10	C1	SC	95	18.36	15.6	28.06	12.22	02:29:29
11	C2	SC	88	17.01	16.6	19.11	15.18	02:07:52
12	C3	SC	97	18.70	10.7	30.30	8.15	00:59:57
13	C4	SC	95	18.36	9.5	28.06	6.59	00:14:02
14	C5	SC	97.5	18.84	10	31.25	6.37	00:11:00
15	M1	Sand clay mix	-	16.09	3	23.94	3.04	00:09:10
16	M2	Sand clay mix	-	15.72	4	17.85	2.22	00:08:30

SC – Clayey sand; sand clay mix – a soil material consists of 80% sand and 20% clay by weight

6. ANALYSIS AND DISCUSSION OF RESULTS

6.1 Introduction

This section presents and discusses the results obtained from the flume experiments. The results comprise data and observations on scour depth and bathymetry, flow fields, as well as the extent of embankment erosion. They were determined from measure data, time series photographs, and trends observed in each experiment. Although further research is needed to extend and confirm the results, the results show that embankment soil strength does influence abutment scour and rate of embankment failure.

6.2 Description and Illustration of Experiments

Observations, extensively recorded by means of photographs taken during experiments, revealed how model embankment soil eroded along the embankment spill-slope during the experiments. Embankment erosion began at the embankment spill-slope’s upstream corner where embankment soil was exposed to the highest values of flow velocity and turbulence. The high velocities and turbulence were due to flow constriction as flow passed around the abutment. The embankment soil failure then continued toward the middle portion of the spill-slope face and further progressed downstream. This process was marked by the formation of undercut, exposed vertical blocks of embankment soil, whose failure occurred relatively quickly as the spill-slope face began eroding and then slowed as spill-slope erosion increased the area of flow at the abutment and reduced flow velocities. Embankments with higher shear strength required longer time to be eroded, and failure was observed with bigger blocks.

The Moultrie camera, programmed to capture photographs every 10 seconds, recorded how the soil blocks failed. It recorded how tension cracks developed due to undercutting and then how the blocks formed and subsequently failed in the toppling mode. A number of additional photographs that were taken manually also visually recorded the formation of tension cracks. Figure 6.1 through Figure 6.4 show measurements (in meters) of failed block size comparing embankment soil position between two consecutive photographs from a fixed reference point. The tension cracks ranged from 10 mm to 30 mm (about 0.5 to 1.25 in.) in distance back from the spill-slope face. As recorded with the photographs, the final shape of the eroded spill-slope (at the time when the experiments ended) was essentially identical for all the experiments.

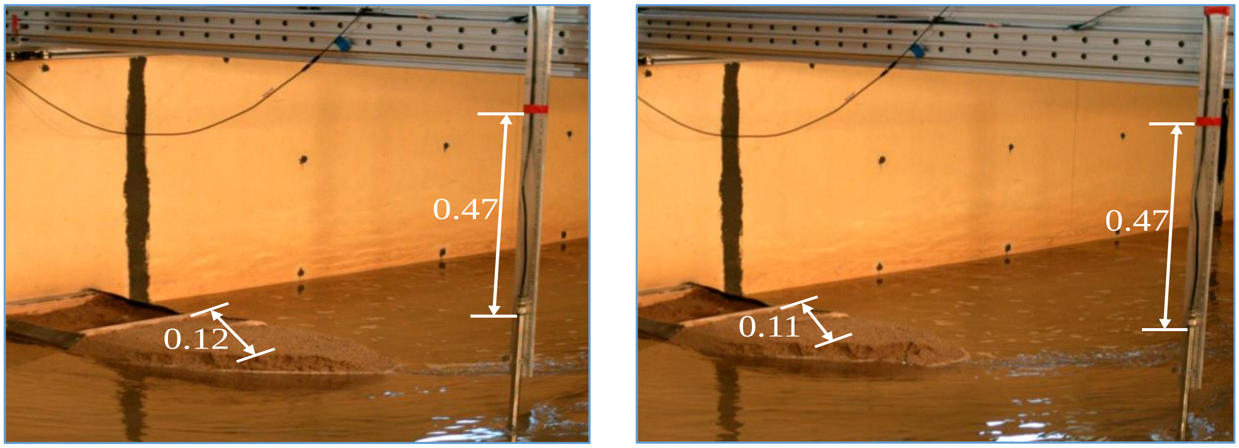

a) b)

Figure 6.1 Block failure size of 1.0 cm recorded in experiment S1 (effective shear strength of soil was 6.73kPa) measured (units in meter) using relative position of soil block in two consecutive time series photographs a) and b); indicated lengths are meters

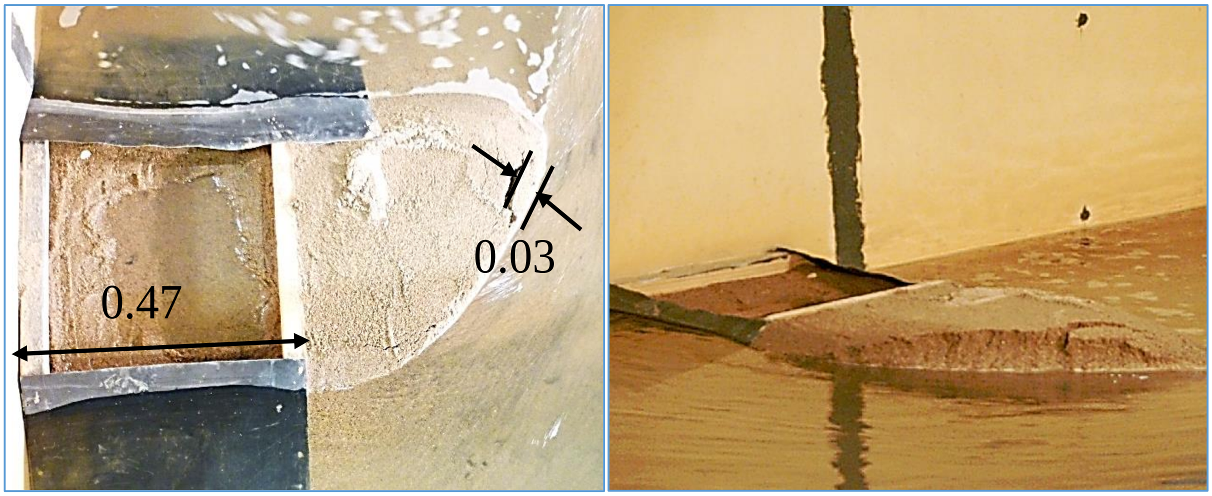

a) b)

Figure 6.2 a) Top view showing the 3.0 cm block failure size; and, b) side view showing dislodged block observed in sand embankment experiment (S3) (effective shear strength was 5.3kPa)

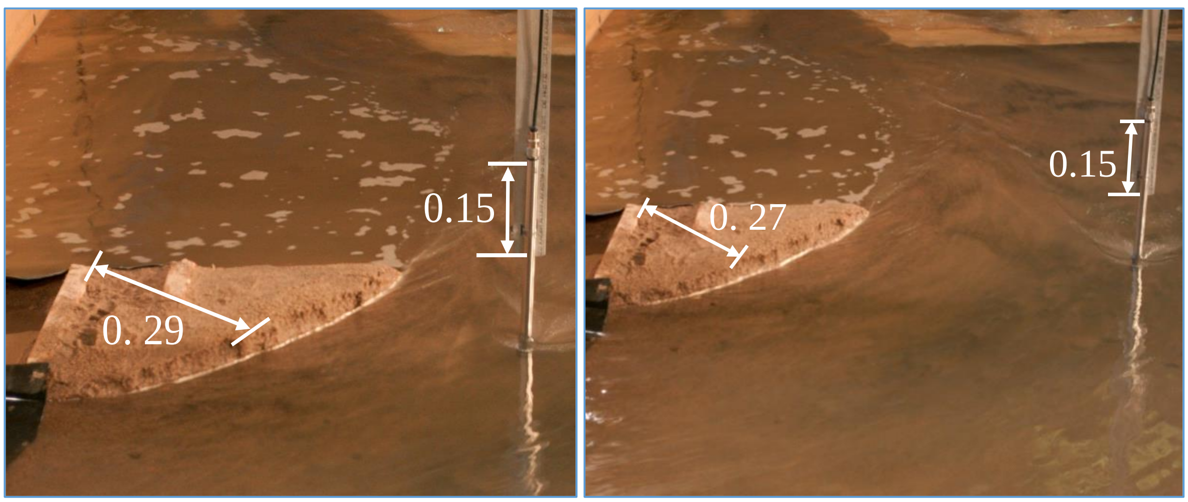

a) b)

Figure 6.3 Block failure size of 2.0 cm recorded in experiment S4 (effective shear strength of soil was 9.45kPa) measured (units in meter) using relative position of soil block in two consecutive time series photographs a) and b).

a) b)

Figure 6.4 Block failure size of 3.0 cm recorded in experiment S6 (effective shear strength of the soil was 8.41kPa) measured (units in meter) using relative position of soil block in two consecutive time series photographs a) and b).

The series of photographs shown in Figure 6.5 to Figure 6.9 illustrate flume experiments with embankments formed of a non-erodible metal plate, erodible uniform sand, clayey sand, and mixed soil, respectively.

6.2.1 Non-erodible embankment

The non-erodible embankment formed of a metal plate had a 200 mm rip-rap blanket placed around the toe[M1] along the circumference as shown in Figure 6.5a. Immediately after the experiment started, turbulence (Figure 6.5b) was observed at the front face of the embankment spill-slope. The bed sand was transported by the flow in a definite path as shown in Figure 6.5c and d. A significant depression region was detected at the same location where the flow turbulence occurred as shown in Figure 6.5e. The scour depth (10.14 cm) for this experiment was highest compared with the depths resulting from all the other experiments.

a) Initial condition; no flow (t = 0 sec)

b) Immediately after the experiment started (t = 30 sec)

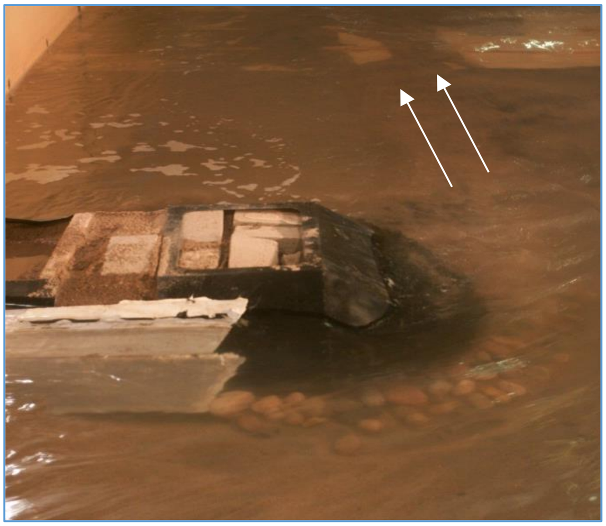

c) Bed material transported downstream follows the path as indicated all the time (t = 11 min)

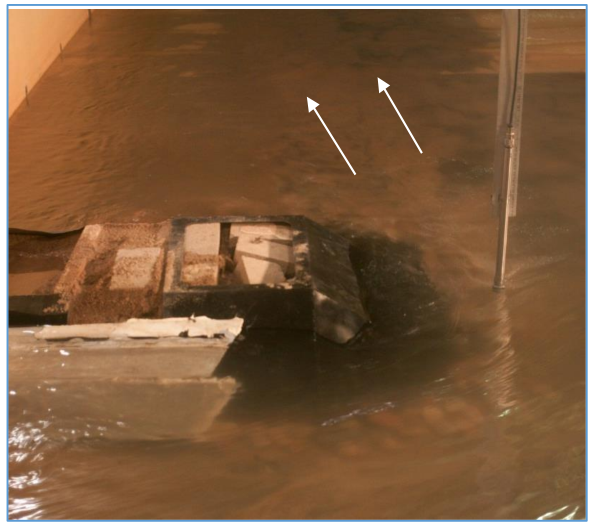

d) Continued scour (t = 37 min)

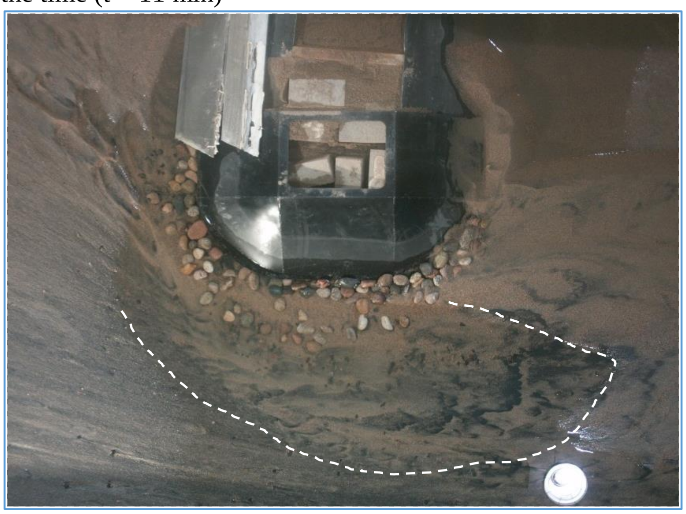

e) The final scour observed once water was drained from the flume. The dashed line shows the maximum aerial extent of scour (t = 50 min 24 sec)

Figure 6.5 Process during flume experiment (M1) for non-erodible embankment formed of metal plate

6.2.2 Embankment formed of uniform sand

The process of undercutting and toppling failure of embankment soil, as discussed in Section 6.2, was observed in the embankment formed of sand. The flume experiment S4 is used as an illustration in Figure 6.6. The embankment soil has effective shear strength of 9.45kPa, and the maximum scour depth developed was 3.63cm. Figure 6.6a shows a uniformly compacted sand embankment. The toppling failure of sand in blocks is demonstrated in Figure 6.6b. The experiment ended once the wood was exposed (Figure 6.6c). A nearly vertical sand embankment (Figure 6.6d) was stable until a tension crack due to undercutting was developed and collapsed the model soil into the flood plain. The maximum scour depression was observed in the leading region of abutment spill-slope as shown in Figure 6.6e.

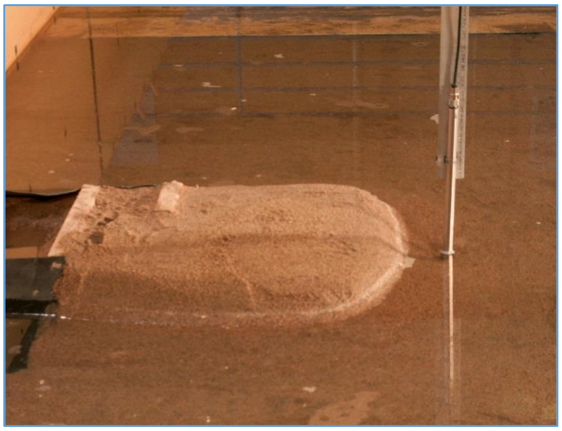

a) Initial condition, no flow (t = 0 sec)

b) Embankment sand block toppling into the flow (t = 3 min)

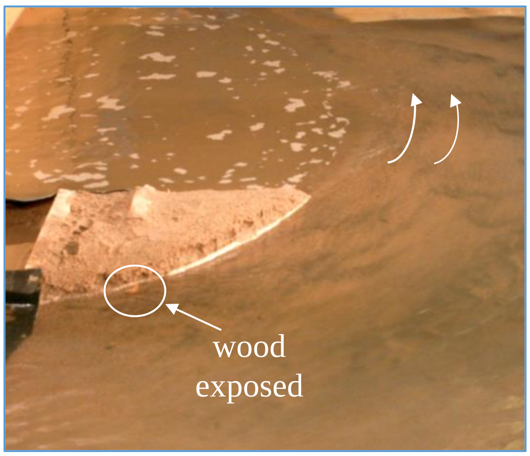

c) Indicator wood exposed and experiment ended (t = 10 min 46 sec)

d) Approx. 45 mm near vertical sand embankment formed before undercutting and collapse

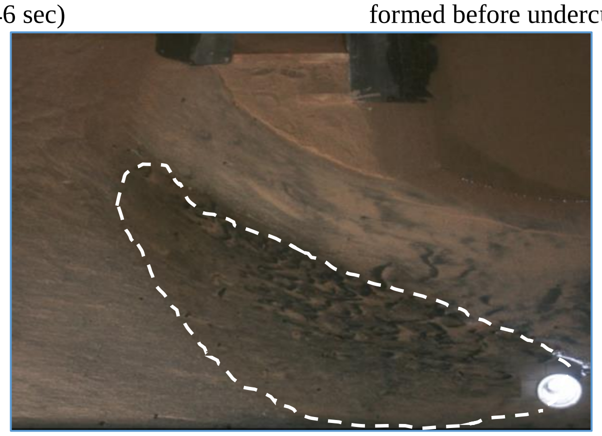

e) Top view of test section after the end of experiment, showing the region of maximum scour of the floodplain bed (maximum scour depth observed in this experiment was 3.63 cm)

Figure 6.6 Processes during flume experiment (S4) for erodible sand embankment

6.2.3 Embankment formed of clayey sand

The shear strength of the cohesive clayey sand embankment could not be controlled adequately for this experiment, and therefore the resulting erosion of the embankment did not simulate the erosion and failure of prototype abutments. Also, the eroded cohesive soil particles mixed with water, which made the water muddy and the erosion process below water level difficult to observe. Nevertheless, this experiment produced useful insights into the erosion of a clayey-sand soil exposed to flowing water as in the present experiment arrangement.

As with the sand embankment, erosion started at the upstream corner of the spill-slope where flow velocity was greatest as shown in Figure 6.7a. The scour hole enlarged with time (Figure 6.7b), and led to loss of support and eventually soil block failure on a large extent as shown in Figure 6.7c. As with the sand embankment, failure of the embankment of clayey-sand started at the upstream spill-slope and progressed downstream. The process now though was prolonged, resulting in the failure of a large block as shown in Figure 6.7d. This failure, illustrated in Figure 6.7e, shows the rotation of embankment soil in a single block about a central axis pivot. These observations show how a model soil having too high shear strength can prevent the model-scale flow from failing the model abutment in suitably scaled blocks.

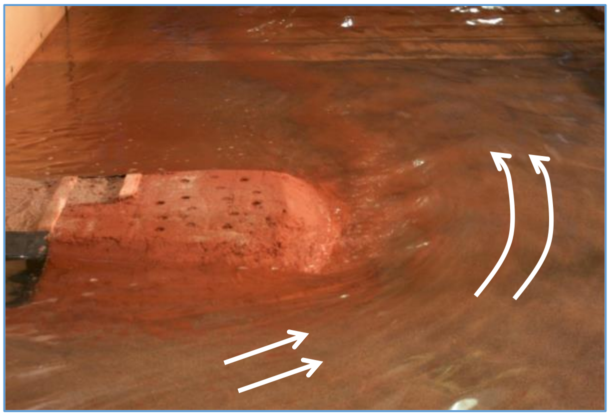

a) Spill-slope erosion at t = 0 sec

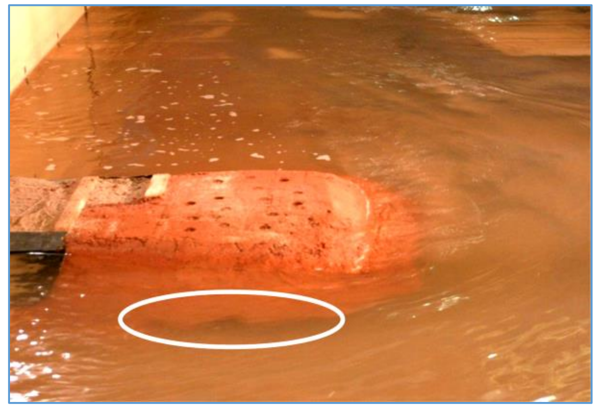

b) Erosion of upstream edge creating a scour hole at t = 6 min

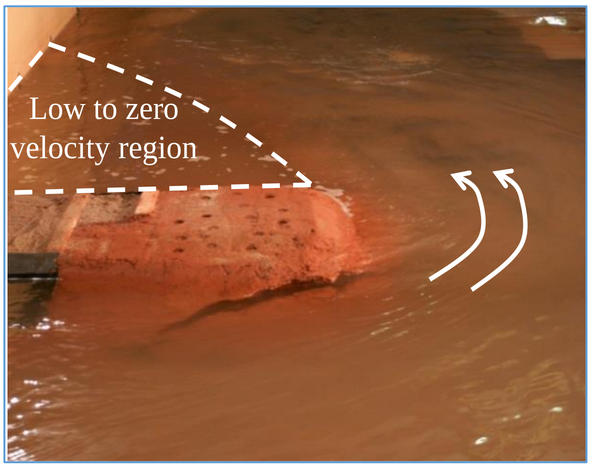

c) Erosion of abutment at t = 12 min 46 sec

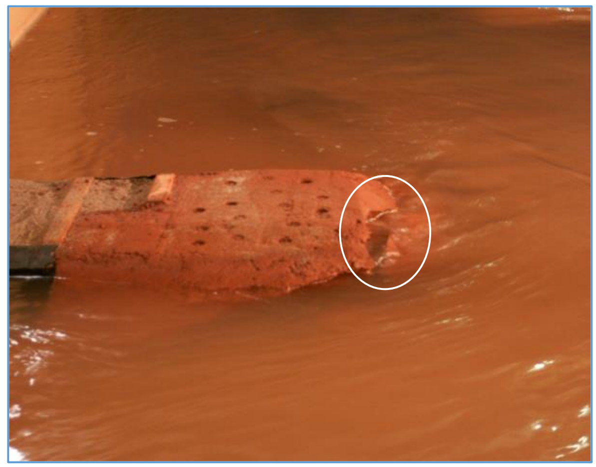

d) Erosion progresses toward downstream at t = 1 hr 19 min

e) Complete failure of model abutment at t = 2 hr 30 min

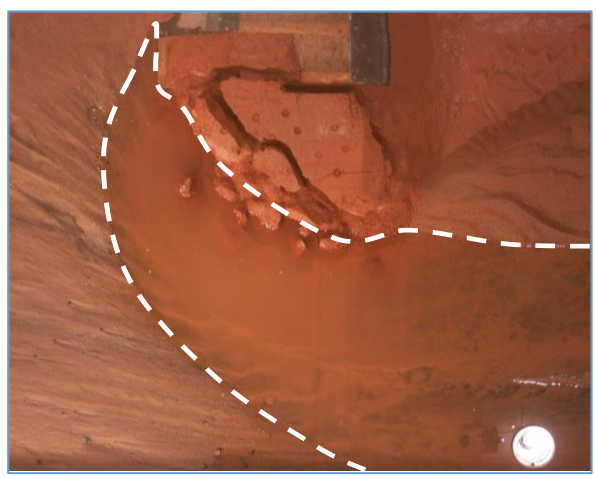

f) Overhead view of failed model abutment (flume drained)

Figure 6.7 Erosion process observed for flume experiment with erodible clayey sand embankment (Experiment C-1)

6.2.4 Embankment formed of mixed soil

The abutment formed of a model soil consisting of a sand clay mix (80% sand, 20% clay), and having effective shear strength 17.85kPa (M2), eroded relatively rapidly, and followed the same process as observed for the abutment formed with sand as the model soil. The resulting maximum scour depth was small compare to depth obtained with the sand, clayey sand, and non-erodible model abutments.

The low maximum scour depth in mix soil in spite of higher effective shear strength than the embankment formed of uniform sand could possibility be due to reducing effective shear strength during scour process. Water could easily flow in and out of uniform sand embankment, for sand being highly porous medium. In case of sand clay mix, water flows in and held by negative charge around clay content. This would reduce effective shear strength during flow as more water penetrates through the embankment soil and accelerate failure. As a result, embankment retreated far before higher maximum scour depth was developed.

Figure 6.8 illustrates the scour and erosion process for this model soil. The maximum scour depth observed for this experiment was 2.22 cm, which was lower than the scour depth in sand although the embankment shear strength was higher. Figure 6.9Figure shows a top view of the test section after experiment ended.

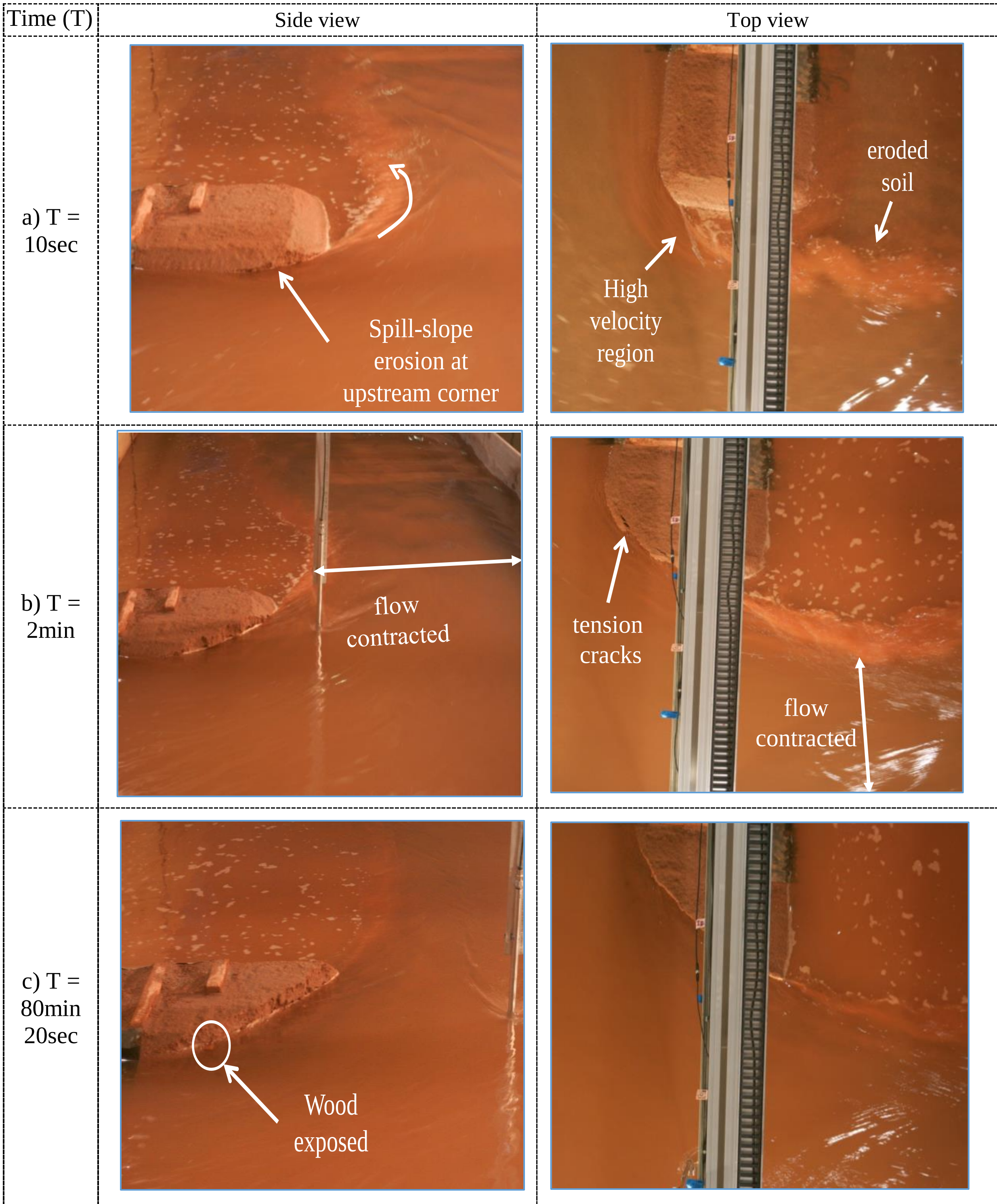

Figure 6.8 Processes during flame experiment (M2) for erodible mixed soil embankment

Figure 6.9 Flume experiment (M2) top view after the experiment ended showing unperceivable bed scour (maximum sour depth observed was 2.22 cm)

6.3 Data Analysis

This section discusses the influences of model soil strength on the rate of erosion of abutment soil and scour depth for the sand embankment. It also briefly describes the procedure for computing the main variables associated with these experiments: a) embankment shear strength, and b) maximum scour depth, analysis of sand bathymetric, and discussion of trends. The sequence of steps described here was followed in the analysis of measurements obtained for each experiment. The general steps are similar for each soil class with a few modifications as mentioned subsequently in this section.

6.3.1 Computation of embankment soil shear strength

The normal stress experienced by the soil particle at the base of the embankment is given by

$$\sigma_v = \gamma_{soil} \times h \tag{6.1}$$

where,
σ_v = normal stress (kPa),
γ_{soil} = the unit weight of compacted embankment soil (kN/m3), and
h = total embankment height (0.2 m)

The total shear strength of model embankment soil for its corresponding normal stress calculated using equation (6.1) was determined from respective correlation charts of each soil class as discussed in Section 4.

Sand has a higher void ratio compared with the other model soils, hence water flows easily into the embankment formed of uniform sand as shown in Figure 6.10. Therefore, porewater pressure (u) develops instantaneously after the flume is filled. As observed in Figure 6.10, the water rose to the top of embankment due to the capillary action building a negative porewater pressure. This would create an apparent cohesion, increasing the shear strength of the sand abutment. It prevented the sliding of the sand block after an undercut.

The effective normal stress (σ') value was computed using equation (6.2). Similar was the case with mixed soil due to a higher percentage (80%) of sand.

The pore size of clayey soil is very small, therefore free water movement into the model soil is interrupted. Compaction further prevents water from flowing into the embankment model. Therefore, no significant porewater pressure is developed. Hence, porewater pressure was considered negligible while computing effective normal strength of the embankment formed of clayey sand using equation (6.2).

The effective normal stress for uniform sand and the sand-clay mix (80/20), were calculated as,\

$$\sigma' = \sigma - u \tag{6.2}$$

where,
σ' = effective normal stress (kPa),
σ = total normal stress (kPa), and
u = porewater pressure (kPa) (determined by equation **Error! Reference source not found.**)).

Porewater pressure at the base of embankment (without considering capillary rise) is given by

$$u = \gamma_{water} \times h_w \tag{6.3}$$

where,
u = porewater pressure (kPa),
γ_{water} = unit weight of water (9.81kN/m^3), and
h_w = water height (0.14m).

a) b)

Figure 6.10 Photographs showing the temporal change in moisture content of the sand abutment: a) during filling the flume; and, b) after the flume is filled. The porewater pressure was developed through capillary action in sand

From the computed effective normal stress, the shear strength of the embankment soil was calculated as explained in Section 4.2.4, 4.3.5, and 4.4.2 for different soil types.

6.3.2 Computation of maximum scour depth

The procedure to obtain a sand bed profile before the pump started or during the experiment is discussed in section 5.3.3. Scour depth was determined by computing the change in the sand bed profile, which represented erosion or deposition along the scan section. The highest value of the change is maximum scour depth, and its corresponding location was also recorded. The same procedure was employed to determine the real time scour during the flume experiments.

6.3.3 Data and trends

a) Non-erodible embankment

Only one flume experiment was conducted using the non-erodible embankment. This abutment model was treated as having infinite shear strength, thereby replicating a rigid abutment made up of concrete or reinforced concrete in real field. The flume experiment with non-erodible embankment was performed to determine the highest scour attainable for infinite embankment shear strength. The observed scour depth was 10.14 cm at location X = -0.13 m (Figure 5.15). The experiment was conducted for 50 minutes and 24 seconds.

b) Uniform sand (SP) embankment

The average duration of the flume experiments with the abutments formed of uniform sand was 8 minutes and 30 seconds. The sand bed erosion rate was higher during the first half of the experiment and then reduced until an equilibrium state was achieved akin to the embankment failure process. The equilibrium was reached by vertical deepening of the channel bed and erosion of the abutment section. Fuller (2012) discovered there was no substantial increase in scour depth by extended test run time once an equilibrium state was achieved. He indicated that the equilibrium state was achieved over a minimum period of approximately 10 minutes. Figure 6.11 is a real time sand bed elevation difference at maximum scour location of flume experiment S1 that characterizes the scour process until the experiment reached equilibrium state, i.e., test section bathometry remained stable.

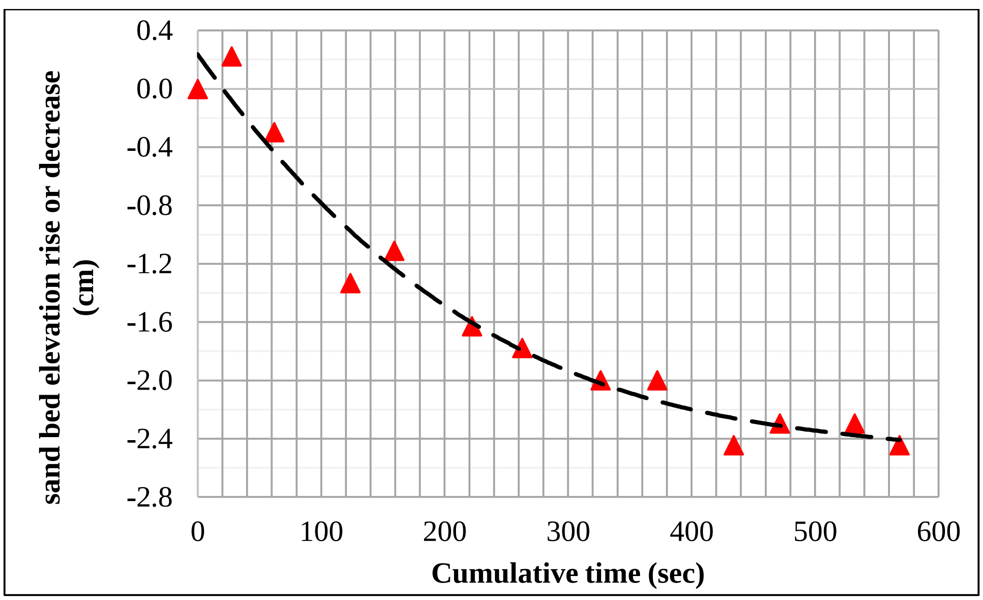

Figure 6.11 Rate of change (scour) of the bed elevation over time, as measured for experiment S1 at the maximum scour depth location

The rate of scour deepening is indicated by the time series of scour profiles in Figure 6.12. The plot shows a full sand bed profile starting at the toe of the embankment along the abutment center line across the test section for various time series. The model sand embankment is represented by a dashed line. The possible source of outliers (demonstrated in Figure 6.12) could be due to a) a change in temperature (which affects the velocity of transducer beam), b) moving sand particles (which created an obstacle and reflect beam before it was an incident on the bed), and c) moving water (disturbs the wave propagation).

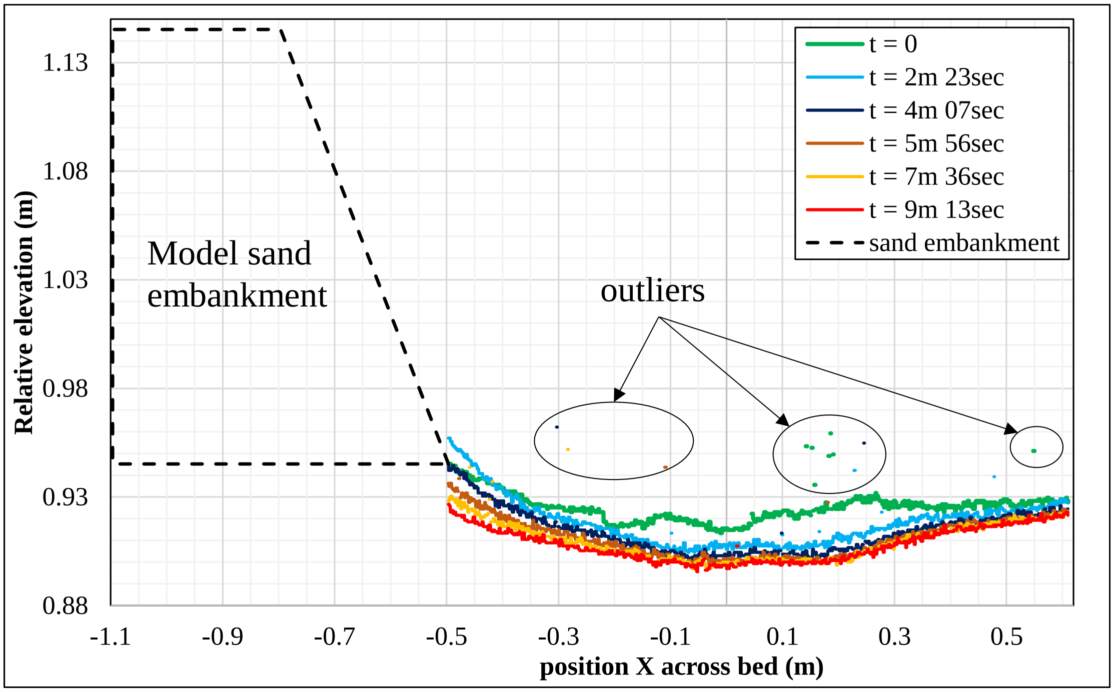

Figure 6.12 Time series scour bed profile of experiment S1

For each of the eight flume experiments performed with the uniform sand abutments (effective shear strengths ranging from 5.3kPa to 9.45kPa), the maximum scour was estimated as the maximum difference in sand bed profiles at start and end of the experiment. Figure 6.13 illustrates a similar process for experiment S1, in which the abutment soil had an effective shear strength 6.73kPa. A 2.44 cm scour depth (d_r) was observed in this experiment.

Data analysis of the scour depths resulting from the range of shear strength values shows that embankment shear strength influences scour depth. It was found that a 50% increase in scour depth occurred in response to a 78% increase in soil shear strength. This finding concurs with the observation that the stronger embankments failed more slowly, thereby increasing the time available for bed scour. When the embankment did not erode, as represented by a metal plate abutment, the scour depth was the highest (see the dashed line in Figure 6.14 for the non-erodible embankment).

The change in scour depth was minimal for values of soil shear strength less than 7kPa (Figure 6.14), owing to the relatively rapid sequence of sand block formation and collapse, causing the spill-slope to retreat faster and, correspondingly, the flow velocities to decrease around the abutment.

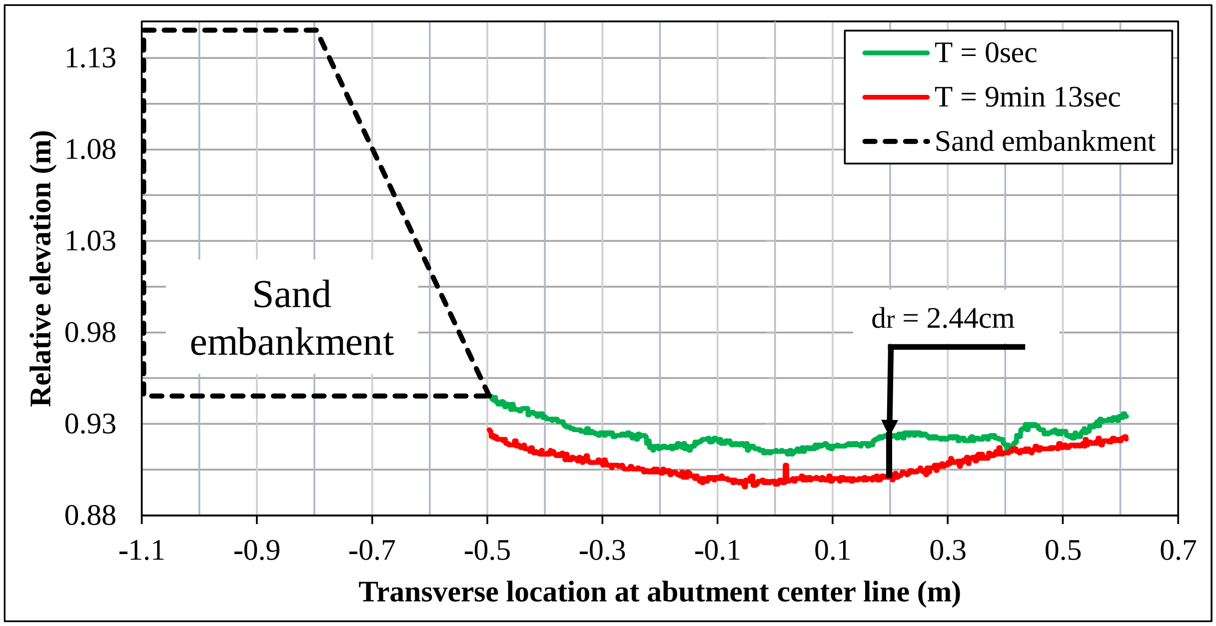

Figure 6.13 Plot of initial and final sand bed elevation for experiment S1 and effective shear strength 6.73kPa

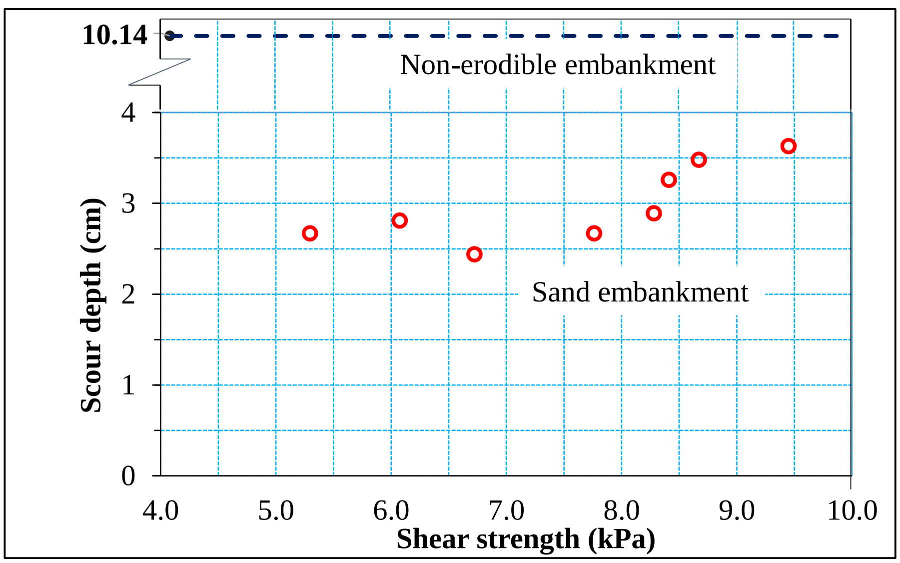

Figure 6.14 Relation between soil shear strength and maximum scour depth for flume experiments formed of uniform sand and non-erodible (dashed line) embankment

The scour-depth data obtained for the non-erodible embankment and the erodible uniform sand abutments are plotted for corresponding soil shear strength in Figure 6.15. A log scale is used for soil strength in order to position the data in the much wider range of strengths associated with soils. The data obtained with the sand present an upward trend, thereby demonstrating a relationship between scour depth and abutment shear strength. Table 6.1 is a summary of the data obtained with the sand abutments.

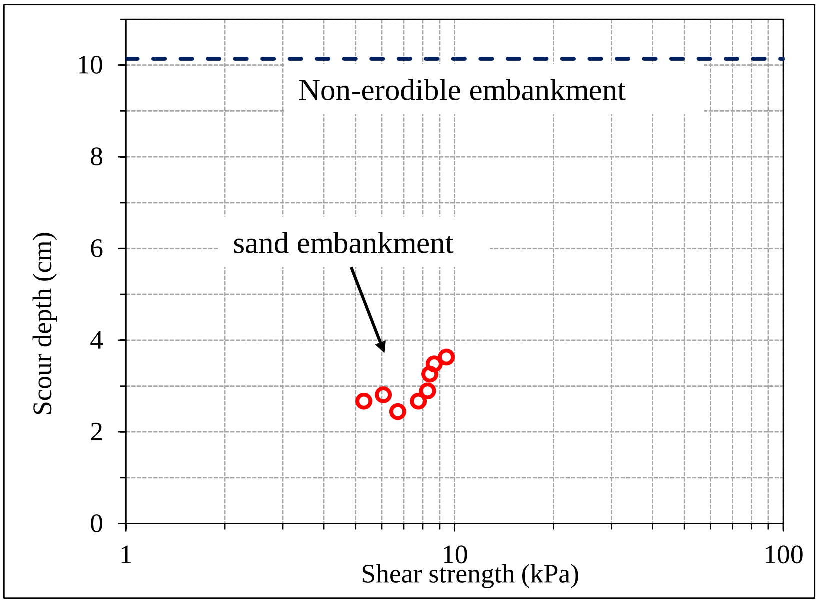

Figure 6.15 Relation between soil shear strength plotted in log scale and maximum scour depth for flume experiments formed of sand and non-erodible (dashed line)

Table 6.1 Summary of data from the experiments with the uniform sand abutments

Expt. No	Relative density %	Unit weight kN/m^3	Avg. Penetration resistance kPa	Moisture %	Effective shear strength kPa	Scour depth cm	Run time hh:mm:ss
S1	62	15.66	289.38	2.83	6.73	2.44	0:09:13
S2	74	16.06	451.98	3.56	8.28	2.89	0:08:26
S3	51	15.31	157.09	4.8	5.30	2.67	0:07:59
S4	83	16.38	609.08	3.36	9.45	3.63	0:10:46
S5	77	16.17	509.86	2.75	8.67	3.48	0:09:54
S6	75	16.10	468.52	1.96	8.41	3.26	0:08:44
S7	57	15.50	231.50	1.68	6.08	2.81	0:07:25
S8	70	15.93	394.11	2.69	7.76	2.67	0:08:25

c) Clayey sand (SC) embankment

The trend in scour depths obtained with the model abutments formed of clayey sand appears to indicate that scour depth reduces as embankment shear strength increases. This finding reflects the influence of numerous variables like moisture content, clay content, particle size affecting soil strength, and erodibility that make the data difficult to compare. Further investigation in which these variables are better controlled is necessary in order to better understand the shear strength versus scour depth relationship for this soil category. These experiments, therefore, should be considered as preliminary in nature. The ensuing paragraph briefly assesses the differences in how these model soils were formed for the experiments.

The five experiments involving the clayey-sand model soils were performed with values of soil compaction ranging from 88% to 97.5% of Maximum Dry Density (MDD). In turn, these compaction values produced a range of soil shear strengths varying from 19kPa to 31kPa. A combination of variables was covered in the flume experiments using SC soil. The experiments included two abutment spill-slopes formed of SC soil passing No. 10 sieve size compacted at the wet side of compaction curve (C1 and C2), one using SC soil passing No 4 sieve size and compacted at dry of compaction curve (C4), two experiments at OMC with each SC soil passing No 4 and 10 sieve size, respectively (C3 and C5). The laboratory tests on the dry side of compaction could not be performed in the Proctor mold as described in section 4.3.4, but flume experiment C4 using the abutment spill-slope formed of SC soil compacted at the dry side of compaction was performed to understand the effect of moisture content on scour depth. TableTable 6.2 summarizes the experiments using SC soil as the abutment soil.

Figure 6.16 relates measured values of maximum scour depth to embankment strength for clayey sand. It was observed that the scour depth was significant for the abutment spill-slope having a relatively high moisture content. However, other variables like particle size, clay content, and uniformity in compaction also affect the embankment erodibility and scour duration, which are not considered during the flume experiments formed of clayey sand.

Table 6.2 Summary of flume experiments using SC abutments spill-slope

Exp. No	Compaction %	Unit weight kN/m^3	Moisture content %	Shear strength kPa	Scour depth cm	Location At X = m	Test time hh:mm:ss	Remarks
C1	95	18.36	15.6	28.06	12.22	-0.3	02:29:29	wet side/ passing # 10 sieve
C2	88	17.01	16.6	19.11	15.18	-0.23	02:07:52	wet side/ passing # 10 sieve
C3	96.75	18.70	10.7	30.30	8.15	-0.26	00:59:57	OMC/ passing # 4 sieve
C4	95	18.36	9.5	28.06	6.59	-0.49	00:14:02	dry side/ passing # 4 sieve
C5	97.5	18.84	10	31.25	6.37	-0.49	00:11:00	OMC passing # 10 sieve

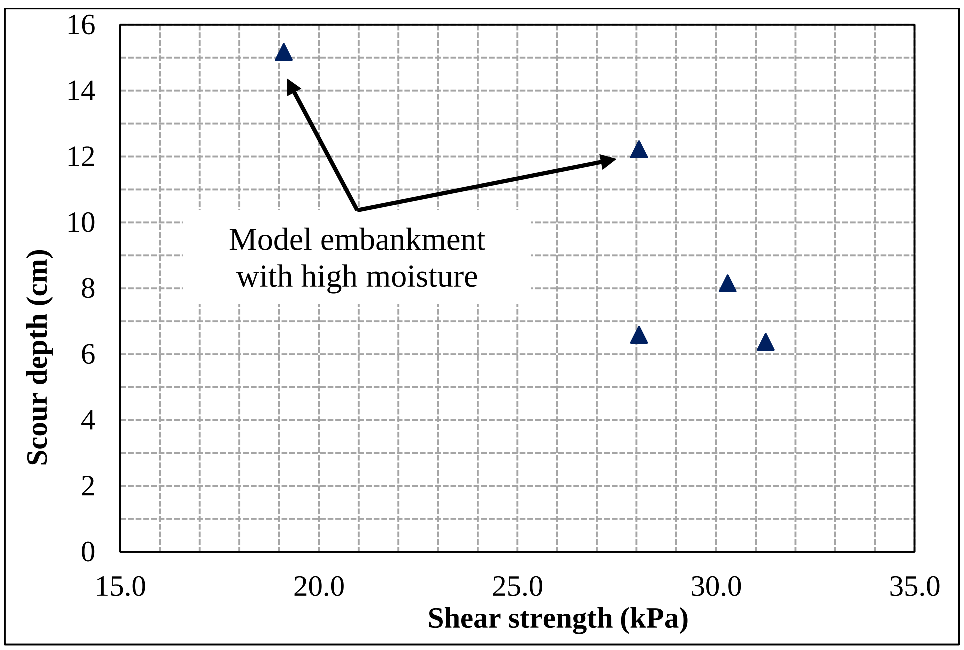

Figure 6.16 Plot of scour depth versus shear strength for the SC model abutments

d) Sand clay mix embankment

The flume experiments with abutments formed of soils characterized as a sand clay mix (80% sand, 20% clay) remained inconclusive as only two experiments were conducted; too few to define a trend. The two experiments involved model soils with effective shear strength values of 17.85kPa and 23.94kPa. The scour depths increased for the stronger soil. The hydraulic-geotechnical failure process observed was similar to that for the abutments formed of uniform sand.

The general trend observed during flume experiments formed of uniform sand, clayey sand, and sand-clay mix indicates that the scour depth increases as abutment soil strengthens. As shown in the summary plot in Figure 6.17, a trend is evident in the data for the uniform sand. More study needs to be carried out in the sand-clay mix to generate more points so as to define a trend. The two high values in clayey sand were for such soils with high moisture content. This finding suggests that further experiments require closer consideration of soil moisture content in model soils formed using clay and sand.

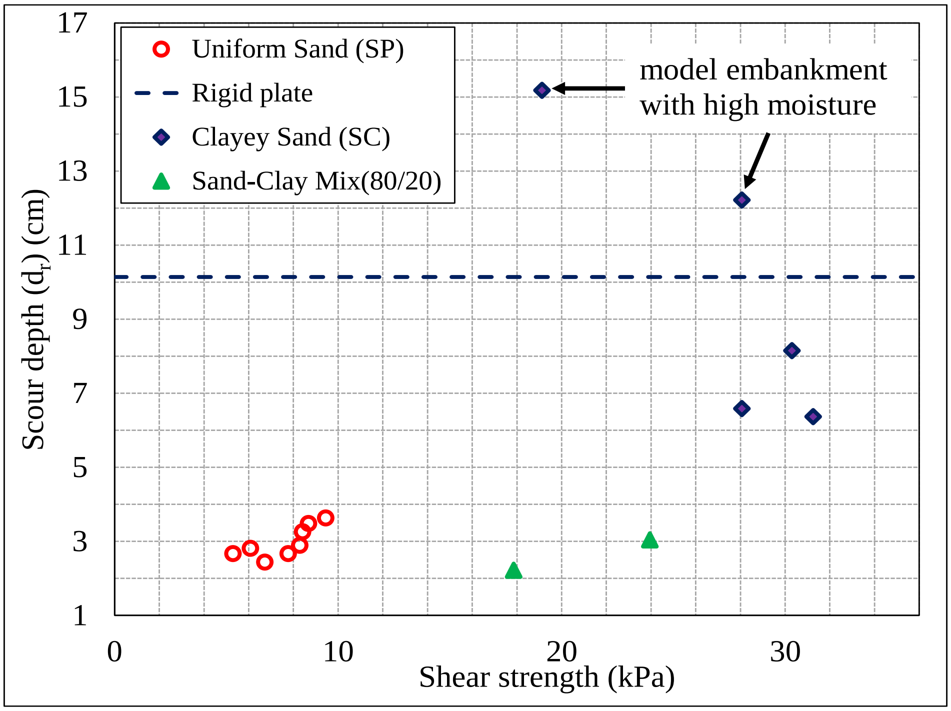

Figure 6.17 A summary plot of scour depth versus soil shear strength

6.4 Large Scale Particle Image Velocimetry Analysis

Large Scale Particle Image Velocimetry (LSPIV) is a relatively easy technique used to produce two-dimensional vector fields of flow velocity on the surface of flow. The principal contributions of LSPIV analysis in this study are determinations of average velocities at the beginning, middle, and end of an experiment. These data documented high velocity regions, location of stagnant regions, reverse flows, turbulence structures, and contraction zone during flow at different time intervals.

6.4.1 Introduction

LSPIV is a flexible, reliable, and economically efficient technology that can be employed at an area of interest for a uniform or non-uniform flow. It is an image-based technology that provides free surface velocity measurements using displacement of floating fluid-markers (seeded material) between successive digital images.

6.4.2 Experimental setup

The flume setup and flow were discussed in Section 5. The analysis was carried out only for the uniform sand abutment model. Video recording was carried out using a SONY Digital HD video camera located directly overhead, shooting down vertically on the test section. The location of the recorder was kept constant throughout the experiment. Packing peanuts (starch foam) and dish soap were used as seeding materials as shown in Figure 6.18. The use of these peanuts created soap bubbles that could easily be detected during the analysis. The experiment was continued until wood was exposed. No scour depth measurement was carried out during LSPIV.

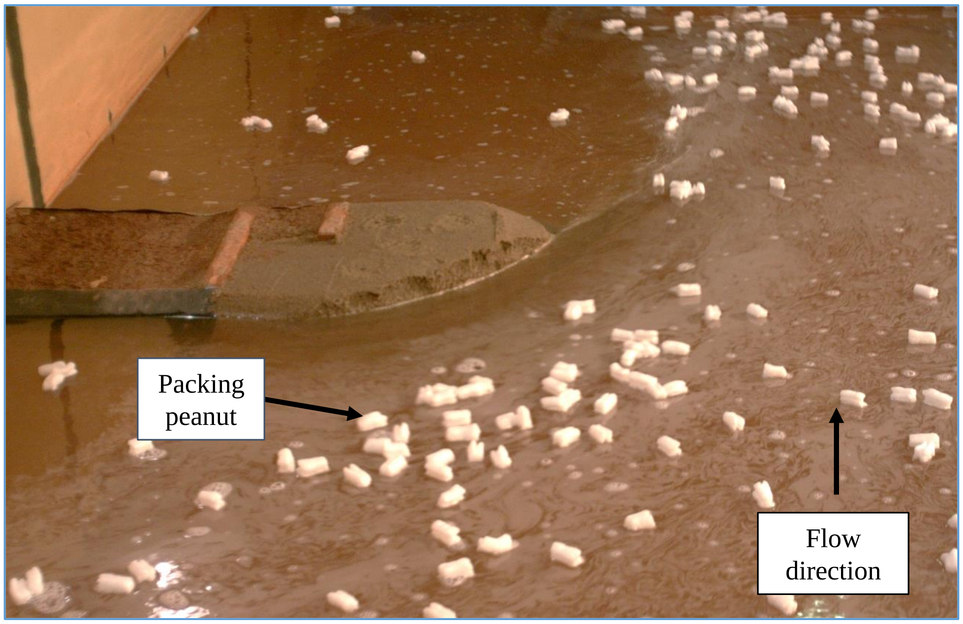

Figure 6.18 View of the model abutment showing the packing peanut (starch foam) used as seeding material for the study

Four benchmarks were positioned on the wooden posts using black tape, as shown in Figure 6.19, as the ground control point. The units are in centimeters.

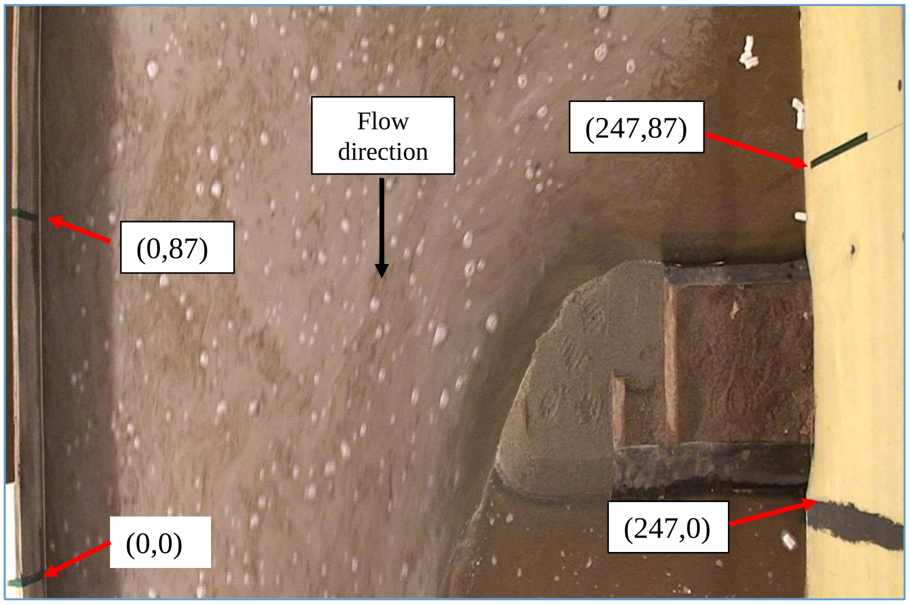

Figure 6.19 Four ground reference points (reference coordinates) used for LSPIV

6.4.3 Analysis

a) Image processing and transformation

Three segments of videos at a time interval of 10 seconds at the beginning, in the middle, and at the end of the flume experiment were downloaded onto the computer using Adobe Premier Pro, which was digitized into a number of separate images at a rate of 30 frames per second.

b) Mat_LSPIV software

Mat_LSPIV software, a graphical user interface in MATLAB, was used to process the digitized images to compute the velocity field vectors. For a detailed procedure on analysis using Mat_LSPIV, "Large-Scale Particle Image Velocimetry for Resolving Unsteady Flow Features at Cylinders" by Basnet and Ettema (2011), can be referred to but is not discussed here.

The final plots are shown in Figure 6.20, Figure 6.21, and Figure 6.22, which show higher velocities at the section where abutment spill-slope obstructs the flow. The velocity at the end (near X = 0) is almost constant due to the contact to the solid wood. At the upstream region near the abutment spill-slope, the velocity increased during the start of the experiment, which later on became almost constant in two subsequent sets of analysis (middle and end of experiment) due to flow relaxation by spill-slope erosion and channel widening. The flow contraction due to obstruction was at the location of the embankment (Figure 6.20) that shifted its location toward downstream as the spill-slope was eroded (Figure 6.22).

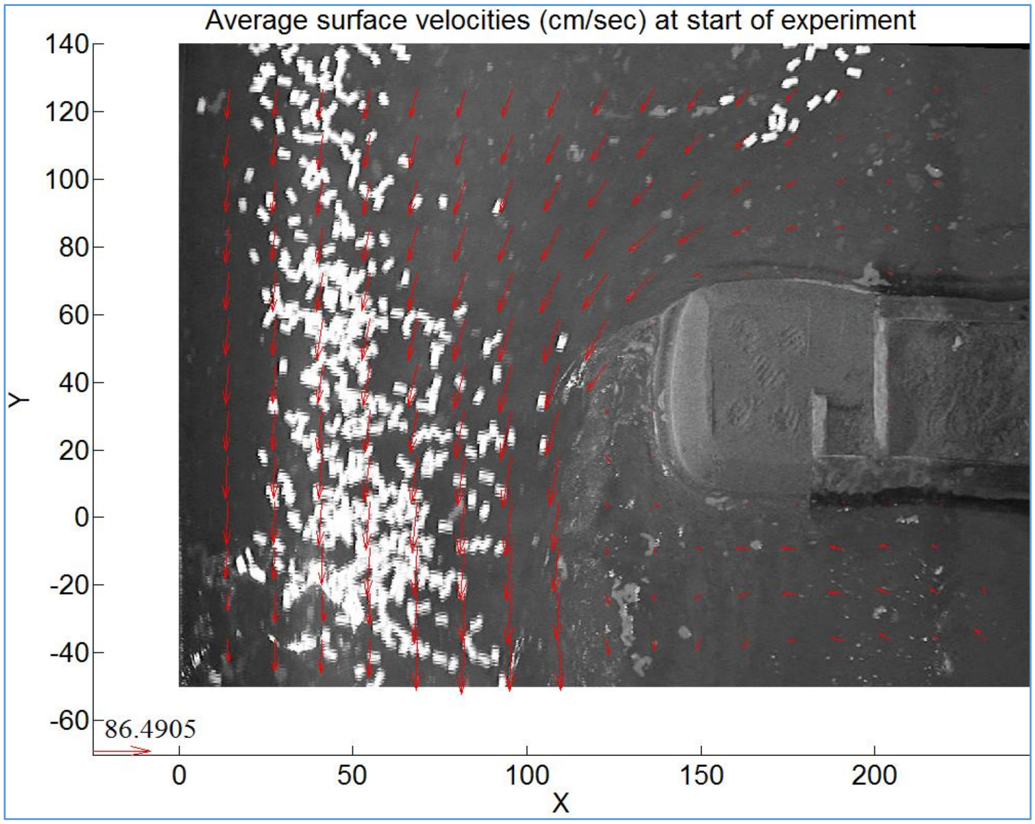

Figure 6.20 Overhead view of the model abutment showing the LSPIV-derived values of surface velocities at the beginning of flume experiment

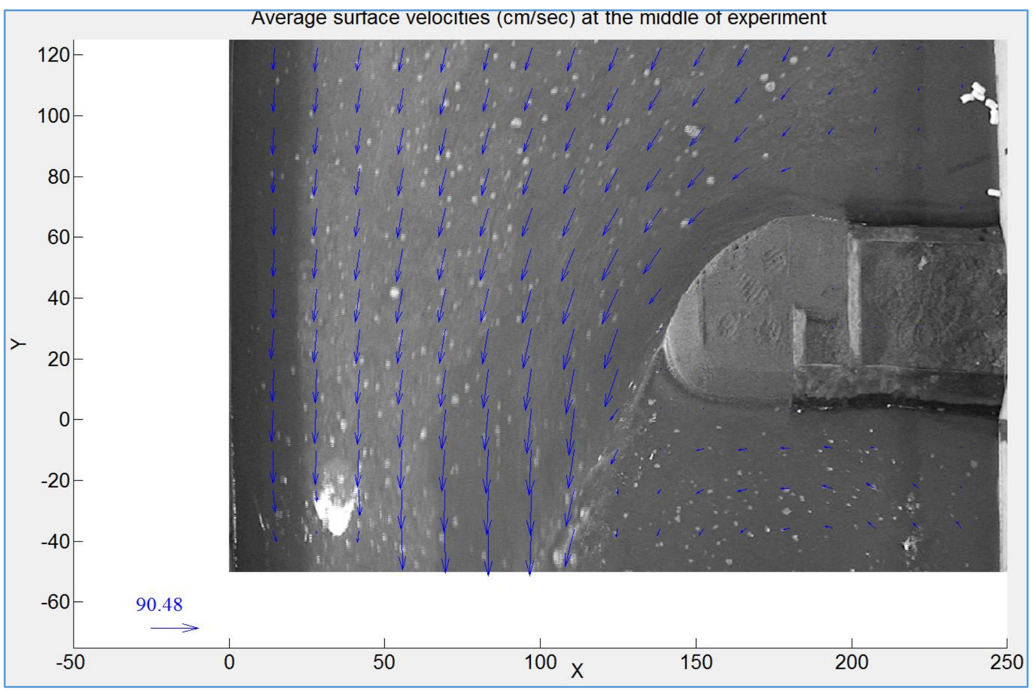

Figure 6.21 Overhead view of the model abutment showing the LSPIV-derived values of surface velocities at the middle of flume experiment

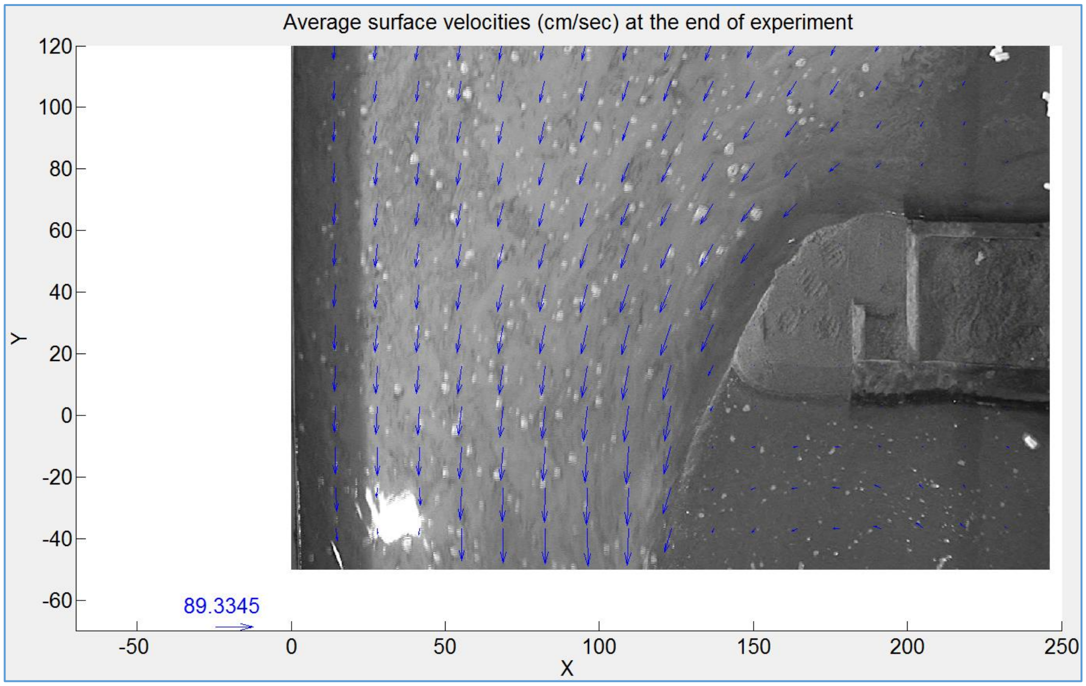

Figure 6.22 Overhead view of the model abutment showing the LSPIV-derived values of surface velocities at the end of flume experiment

7. CONCLUSION AND RECOMMENDATIONS

7.1 Introduction

The main contributions of study MPC 354 are insights into the processes whereby spill-through abutments, especially their spill-slopes, fail during abutment scour, and how abutment and spill-slope soil strength affects abutment failure and scour depth. These insights were obtained from flume experiments using model abutments formed of compacted uniform sand. Additional preliminary analysis of model abutments formed of clayey sand and sand clay mix indicated greater complexity of behavior and the need for further investigations.

This final section presents the main conclusions drawn from the present study. It also presents recommendations regarding aspects of scour requiring further investigation.

7.2 Conclusions

Although abutment failure involves geotechnical failure of the abutment's earthfill spill-slope and embankment, geotechnical influences on scour have received little prior investigative attention, partly because of difficulties in scaling and quantifying the geotechnical properties of soil used for a model spill-slope and embankment. As a result, the leading design guides do not address the influence of geotechnical properties of spill-slope and embankment soil on scour.

The present study led to the following new insights regarding geotechnical effects on abutment scour:

a) The scour depths obtained with erodible abutments flume experiments were substantially less than that obtained when the model abutment was rigid and resistant to erosion. The maximum scour depth obtained with the sand abutment was only 40% of that resulting with the rigid abutment.

b) A combination of geotechnical and hydraulic processes interacted in eroding the compacted earthfill spill-slope of bridge abutments. Consequently, geotechnical properties can significantly affect the overall scour process, lead to abutment failure, and limit depth of scour in the channel adjoining the abutment.

c) Under-cutting, the development of tension cracks due to loss of support, and the subsequent toppling of soil blocks occurred sequentially along the face of the spill-slope, starting at the upstream where the velocity is highest. This process eroded the spill-slope, and eventually exposed the abutment column. Further erosion would then result in breaching of the embankment.

d) The approximate failure block size observed in the scale-reduced flume model was around 1 cm to 3 cm, which replicates block sizes around 0.3 m to 0.9 m at prototype abutments (the model replicated a standard single-lane road at a length scale of 1:30).

e) The scour depths measured near the model abutments formed of sand compacted to a range of unit weights were found to correlate with soil shear strength, although only when soil strength exceeded a value of about 8.0kPa. For soil strengths less than this value, scour depths varied little with soil strength. This trend occurred largely because the strength of the spill-slope soil was difficult to control consistently for the less compacted sands. For soil (sand) strengths above 8.0kPa, scour depth increased with increasing soil (sand) strength. Also, the rate of spill-slope erosion slowed as soil strength increased.

f) Scour of the channel bed (or flood plain) around the abutment developed simultaneously as the abutment eroded, with the flow causing adjustments (reduction in velocity) in scour as the abutment eroded. Abutment erosion increased the cross-sectional area of flow across the abutment center-line and correspondingly reduced the overall average velocity of flow. Although scour of the channel bed and abutment erosion are coupled, scour development in the channel occurred at a rate and time scale indirectly linked to abutment erosion.

7.3 Recommendations for further study

The essential geotechnical process occurring during abutment scour is highly three-dimensional and is affected by soil properties. Laboratory investigation of this process is complicated due to difficulties in quantifying and controlling the strength properties of scaled embankment model. A carefully controlled procedure for compaction of model sand during laboratory tests and flume experiments is required, as are means for accurately measuring of model soil strength. The following recommendations will improve these considerations in future experiments on scour at erodible abutments:

1. Further experiments are needed using stronger model soils than were used in the present study. These experiments will complete the curve shown in Figure 6.17.

2. A better compaction procedure should be developed to build model embankments and spill-slopes so as to have controllable soil strengths. The consistent compaction in number of layers should be conducted to produce embankments of uniform strength. Careful attention should be given to forming the model spill-slope as its changing thickness and curvature can make it especially difficult to build.

3. A correlation method was adopted in the present study to determine the strength of compacted embankment soil in the flume. However, this indirect method is not efficient as it accumulates errors during development of the correlation chart. One source of error is the relatively small amount of data used to develop the correlation. A more efficient procedure would be to use an instrument that directly measures the shear strength in flume experiments. One of the good options is the use of a Cone Penetration Test customized device, which is discussed in Section 3.2[M2]. This instrument would make it easier to conduct experiments with a broader range of soil strengths.

4. Some further developments in instrumentation used are needed. For example, the two different output data produced by two programs controlling the carriage-mounted acoustic transducer and instrument beam could be coupled together by a single program that controls both instruments and develops one output. This development would save time during analysis and remove interpolation induced errors.

5. Acquisition of the sand bed bathometry of the whole test section could be obtained in a future study, as this information would expand the limitation of analyzing the maximum scour depth along the abutment center line.

6. Field verification of the results obtained from flume experiments will help confirm the processes observed and measured in the present laboratory experiments.

REFERENCES

Arneson, L.A., Zevenbergen, L.A., Lagasse, P.F., and Clopper, P.E. (2012). *Evaluating Scour at Bridges*. Fifth Edition. Report No. FHWA-HIF-12-003, Hydraulic Engineering Circular No. 18, Federal Highway Administration, U.S. Department of Transportation, 340 p.

Basnet, K. and Ettema, R. (2011). "A Large-Scale Particle Image Velocimetry for Resolving Unsteady Flow Features at Cylinders." *Proceedings of the 34th IAHR World Congress, Brisbane, Australia*, pp. 3378-3387.

Baxter, C., Sharma, R., Seher, N., and Jander, M. (2010). "Evaluation of Liquefaction Resistance of Non-Plastic Silt From Mini-Cone Calibation Chamber Tests." *Proceedings of the 2nd International Symposium on Cone Testing*, CPT-10, 8 p.

Chakradhar R.S. (2014). *Laboratory Investigation Of Geotechnical And Hydraulic Influences During Abutment Scour*. MS Thesis, Department of Civil and Architectural Engineering, University of Wyoming, Laramie, WY.

Esquivel, E.R., and Silvia, C.H. (2000). "Miniature Piezocone for Use in Centrifuge Testing." *Proceedings of the Geotechnical Special Publication: Innovations and Applications in Geotechnical Site Characterization*, ASCE, Denver, CO, pp. 118-129.

Ettema, R., Nakota, T., and Muste, M. (2010). *Estimation of Scour Depth at Bridge Abutments*. NCHRP 24-20, National Cooperate Highway Research Program, Transportation Research Board, Washington, D.C., 436 p.

Fuller, J.J. (2012). *Geotechnical and Hydraulic Processes during Scour at Spill through Bridge Abutments*. MS Thesis, Department of Civil and Architectural Engineering, University of Wyoming, Laramie, WY.

Hossain, B., Sakai, T., and Hossain, Z. (2010). "River Embankment and Bank Failure: A Study on Geotechnical Characteristics and Stability Analysis." *American Journal of Environmental Sciences*, 7(2), pp. 102-107.

Howard, I.L., and Badran, W.H. (2011). "Comparison of Hand Held Gage and Unconfined Compression Results in Low Strength Cementitious Stabilized Materials." *Proceedings of Geo-Frontiers*, ASCE, Dallas, TX, pp. 2574-2583.

Kurup, P.U., and Tumay, M.T. (1998). "Calibration of a Miniature Cone Penetrometer for Highway Applications." *Transportation Research Record Journal*, No. 1614, Transportation Research Board, Washington D.C., pp. 8-14.

Lagasse, P.F., Clopper, P.E., Pagain-Ortinz, J.E., Zevenbergen, L.W., Arneson, L.A., Schall, J.A., and Girard, L.G. (2009). *Bridge Scour and Stream Instability Countermeasures: Experience, Selection and Design Guidance, Volume I*. Hydraulic Engineering Circular No. 23, Federal Highway Administration, U.S. Department of Transportation, 259 p.

Landers, M.N. (1992). "Bridge Scour Data Management." *Proceedings of Hydraulic Engineering: Saving a Threatened Resource-In Search of Solutions*, ASCE, Baltimore, Maryland, pp. 1094-1099.

Mayne, P.W. (2007). *Cone Penetration Testing*. NCHRP Synthesis 368, Transportation Research Board, Washington, D.C., 126 p.

Melville, W.B. and Coleman, E.S.. (2000). *Bridge Scour*. Water Resource Publications, LLC., Highlands Ranch, CO, 550 p.

Murrillo, J.A. (1987). *The Scourge of Scour*. Civil Engineering, ASCE, 57(7), pp. 66-69.

Osman, A.M., and Thorne, C.R. (1986). "Riverbank Stability Analysis I: Theory." *Journal of Hydraulic Engineering*, 114(2), pp. 134-150

Richardson, E.V., and Davis, S.R. (2001). *Evaluating Scour at Bridges*. Forth Edition. Report No. FHWA NHI 01-001 HEC-18, Hydraulic Engineering Circular No. 18, National Highway Institute, Federal Highway Administration, 378 p.

Sturm, T., Ettema, R., and Melville, B.W. (2012). *Evaluation of Bridge-Scour Research: Abutment and Contraction Scour Processes and Prediction*. NCHRP Web-Only Document 181, NCHRP Project 24-27(02), Transportation Research Board, Washington D.C., 106 p.